

# AKUTAN GEOTHERMAL PROJECT

## Report on 2009 Exploration Activities



**A. Kolker<sup>1</sup>, W. Cumming<sup>2</sup>, P. Stelling<sup>3</sup>, A. Prakash<sup>4</sup>, C. Kleinholz<sup>4</sup>**

<sup>1</sup>AK Geothermal, LLC, Portland, OR

<sup>2</sup>Cumming Geoscience, Santa Rosa, CA

<sup>3</sup>StelCo Magma Consulting, Bellingham, WA

<sup>4</sup>University of Alaska Geophysical Institute, Fairbanks, AK

## Contents

Abstract.....	3
I. Introduction .....	3
II. Background .....	4
1. <i>Thermal manifestations and geochemistry</i> .....	4
2. <i>Structure</i> .....	6
III. Exploration Methods and Results.....	8
1. <i>Geologic reconnaissance and geothermometry</i> .....	8
2. <i>Soil geochemical surveys</i> .....	13
3. <i>Remote sensing</i> .....	16
4. <i>MT survey</i> .....	19
5. <i>Thermal field mapping</i> .....	25
IV. Discussion.....	27
1. <i>Geothermal resource interpretation</i> .....	27
2. <i>Exploratory well drilling</i> .....	32
3. <i>Geothermal development</i> .....	33
V. Conclusions and Next Steps .....	35
References.....	36

*Cover page photos, clockwise from top left: Pete Stelling at the head of Hot Springs Bay Valley; Mark Kitchen, Jesus Barrio, John Tcherpanoff, and Alec Sandberg overlooking Hot Springs Bay; Amanda Kolker hiking in Hot Springs Bay Valley; Alec Sandberg near hot springs group A.*

## **Abstract**

In summer 2009, the City of Akutan executed an exploration program to better characterize the geothermal resource on Akutan Island. The exploration program included practical access assessments, a geologic reconnaissance field study, soil and soil gas geochemical surveys, a remote sensing study using satellite data, a review of existing hot springs geochemistry data, a magnetotelluric (MT) survey, and a conceptual model analysis. Alternative interpretations of the MT and geochemistry data in the context of the geology results were emphasized in preparing a range of resource conceptual models. Two well targets were chosen based on where practical access allowed effective testing of the conceptual resource models.

The most important data for building our conceptual model turned out to be the geochemistry of Akutan hot springs fluids collected prior to the 2009 study; and the results of the 2009 MT survey. The soil geochemistry results and remote sensing results were of lesser utility and serve primarily as background information.

This report presents the results of the 2009 exploration program and discusses the implications for the geothermal resource and its potential development. The next stage of exploration includes access analysis, logistics analysis for drilling, and the completion of two to four wells.

## **I. Introduction**

The geothermal system on Akutan Island is considered one of the most promising high-temperature sites in Alaska for geothermal resource development (Motyka et al., 1993, Kolker 2007), but until recently very little exploration has occurred at the site.

The City of Akutan plans to develop its geothermal energy resource as part of a long-term comprehensive renewable energy strategy. In 2009, the City applied for and received energy grant and loan funds totaling \$3.7 million from the state of Alaska. Part of these funds were used to conduct exploration activities in summer 2009 in order to better characterize the geothermal resource and to target exploratory wells planned for summer 2010.

The 2009 exploration program consisted of coordinated ground-based and remote geoscientific surveys. This report presents the exploration results and discusses the implications for the geothermal resource, the next stage of exploratory drilling, and potential development issues. Exploration activities coordinated with a preliminary economic assessment study of the Akutan Geothermal Project (Information Insights, 2010). A preliminary feasibility study is planned for 2010.

## II. Background

Akutan volcano is part of the Aleutian Volcanic Arc, which is Alaska’s most promising setting for geothermal energy. Fifty-six geothermal systems have been identified in the Aleutian Arc; many more likely exist but remain unknown due to poor surface expression (Motyka et al, 1993). Akutan volcano is one of the most active volcanoes in the Aleutians, with 32 historic eruptions. It is a composite stratovolcano with a summit caldera ~2 km across and 60-365 km deep (Newhall and Dzurisin, 1988; Miller et al., 1998). Most of the reported eruptions included small-to-moderate explosions from the active intracaldera cone. Several fumarolic areas are present along its south and southwest flank (Lu et al., 2000).

### 1. *Thermal manifestations and geochemistry*

Several thermal springs are located in Hot Springs Bay Valley (HSBV). HSBV is located ~6 km from Akutan village and ~4 km from Akutan Harbor, one of the few sheltered, deep-water harbors in the Aleutians. The fumarole field lies between the volcano’s summit and HSBV. Temperatures of the hot springs range from 40-84°C, and fumarole temperatures as high as 99°C have been measured. No drilling has yet occurred at Akutan, so resource parameters are still unknown and must be estimated. A 10 MW plant size was proposed in 1994 based on existing information about the resource potential and projected energy demand for Akutan.

A state-funded exploration program was carried out in Akutan Island in the early 1980s. The exploration effort was limited to the immediate hot springs area and included detailed geologic mapping, shallow (<150m) geophysical surveys, soil and fluid geochemical studies, and hydrologic investigations. The study found that Akutan hot springs fluids were of the NaCl type (sodium chloride) and relatively dilute, with total dissolved solids (TDS) concentrations of <2,000 ppm (Table 1). Exceptions are the Hot Springs group E fluids, which are closest to the bay and appear to be contaminated with seawater; and the acid spring that occurs close to the fumaroles, the chemistry of which is probably controlled by gas condensates.

Sample Name	Temp °C	Li	Na	K	Ca	Mg	SiO2	B	Cl	F	SO4	HCO3	Sr	Fe	TDS
HS A3	84.0	1.3	323	28	12	0.9	145	11	420	1.1	43	172	0.31	0.05	1080
HS A3	84.0	1.2	328	26	12	1	135	12	410	0.9	43	nd	0.32	0.01	nd
HS A3	Nd	1.2	386	26	12.5	0.9	140	10	424	1.1	54	89	nd	nd	1100
HS B1	47.4	0.61	172	16	15	1.5	103	5.9	220	0.6	22	116	0.1	0.57	617
HS C4	73.4	0.61	207	16	18	1.6	135	7	280	1.0	43	118	0.22	<0.01	762
HS D2	58.8	0.34	128	9.3	11	12	91	3.4	140	0.9	26	128	0.09	0.03	481
HS E	67	1.1	1660	74	130	320	121	4.5	3440	0.5	495	161	1.2	0.04	6350
Fum sp	92.3	0.01	17	3.5	13	13	220	<0.5	5.2	<0.1	1300	nd	0.5	nd	1630

*Table 1. Geochemical composition of Akutan hot springs waters (HS groups A-E) and Fumarole acid spring waters (“fum sp”). Analyses from Motyka and Nye, 1988. All concentrations in ppm.*

Flow rates for the hot springs were only measured at group A. At group A, three springs flow at 40, 51, 118 liters per minute, respectively, into Hot Springs Creek. The isotopic composition of Akutan hot springs fluids is given in Table 2.

Sample Name	Temp °C	del O-18	delδ
HS A3	84.0	-9.2	nd
HS A3	84.0	-10.5	-70
HS A3	nd	nd	nd
HS B1	47.4	-10.8	-71.5
HS C4	73.4	-10.8	-71
HS D2	58.8	-9.2	-69
HS E	67	-8.8	-59
Fum sp	92.3	-1.4	-39

*Table 2. Stable isotope data for Akutan hot springs waters (HS A-E) and fumarole acid spring waters (“fum sp”). Analyses from Motyka and Nye, 1988.*

The fumarole field, often referred to as “flank fumaroles,” occurs at an elevation of 350 m, near the head of Hot Springs Bay valley about 3.5 km southwest of the lower valley hot springs (see Fig. 1). The field consists of a series of low- to moderately-pressurized fumaroles, mildly steaming ground, and boiling acid-sulfate springs covering an area of about 5,000 m. (Motyka and Nye, 1988).

Akutan fumarole gasses were sampled as part of the geothermal exploration study (Motyka and Nye, 1988), and again in 1998 in a USGS study (Symonds et al., 2003). The objective of the USGS study was to investigate the origin of volcanic gases (carbon, nitrogen, and noble gases) in discharges from Cascade Range and Aleutian Arc volcanoes (Table 3). Unfortunately, neither dataset is of sufficient quality to be used for reliable gas geothermometry (Table 3).

Sample Name	CO2	H2S	Ar	N2	CH4	H2	He	CO	O2
SY-AK1	58.4	<.008	0.0117	34.4	4.93	nd	0.0001	0.0032154	5.07
SY-AK2	95.6	2.00	0.040	2.10	0.20	nd	0.00068	0.0033666	0.0034
SY-AK3	92.0	6.40	0.0025	1.41	0.14	nd	0.00046	0.0004392	0.006
M-AE11(hs)	10.27	6.26	1.73	76.68	4.58	0.45	0.0012	N/A	N/A
M-AL9(as)	92.53	2.83	0.02	2.96	1.32	0.34	0.0007	N/A	N/A
M-BN4(f)	95.47	1.44	0.009	1.96	0.92	0.20	Tr	N/A	N/A
M-BN14(f)	94.35	1.41	0.021	3.07	0.91	0.19	Tr	N/A	N/A
M-RM3(f)	95.03	1.28	0.097	2.29	1.05	0.21	Tr	N/A	N/A

*Table 3. Gas composition of Akutan fumaroles and hot springs gases. Samples with prefix “SY” from Symonds et al. (2003); samples with prefix “M” from Motyka and Nye (1993). The Motyka and Nye study includes gas measurements from fumaroles (f), fumarole acid-sulfate springs (as) and hot springs (hs). All values in mol %. nd = None detected; Tr = trace; N/A = not analyzed.*

## 2. Structure

In March 1996, a swarm of volcano-tectonic earthquakes ( $>3000$  felt by local residents,  $M_{max} = 5.1$ ) beneath Akutan Island produced extensive ground cracks but no eruption of Akutan volcano. InSAR images that span the time of the swarm reveal complex island-wide deformation, suggesting inflation of the western part of the island and relative subsidence of the eastern part. The axis of the deformation approximately aligns with new ground cracks on the western part of the island and with Holocene normal faults that were reactivated during the swarm on the eastern part of the island. The deformation is thought to result from the emplacement of a shallow, east-west-trending, north-dipping dike plus inflation of a deep magma body beneath the volcano (Lu et al., 2000). Studies of  $^3\text{He}/^4\text{He}$  ratios in Akutan fumarole gasses indicate degassing of relatively fresh near-surface magma ( $>6 R_c/R_A$ ; Symonds et al., 2003). This implies that unlike many other composite stratovolcanoes, Akutan's magmatic plumbing system includes two lateral rift zones, similar to the classic rift zones at Hawaiian volcanoes and elsewhere. These rift zones are aligned along the regional least-compressive-stress axis (John Power, pers. comm.), and serve as active magmatic conduits at shallow crustal depths (Fig. 1).

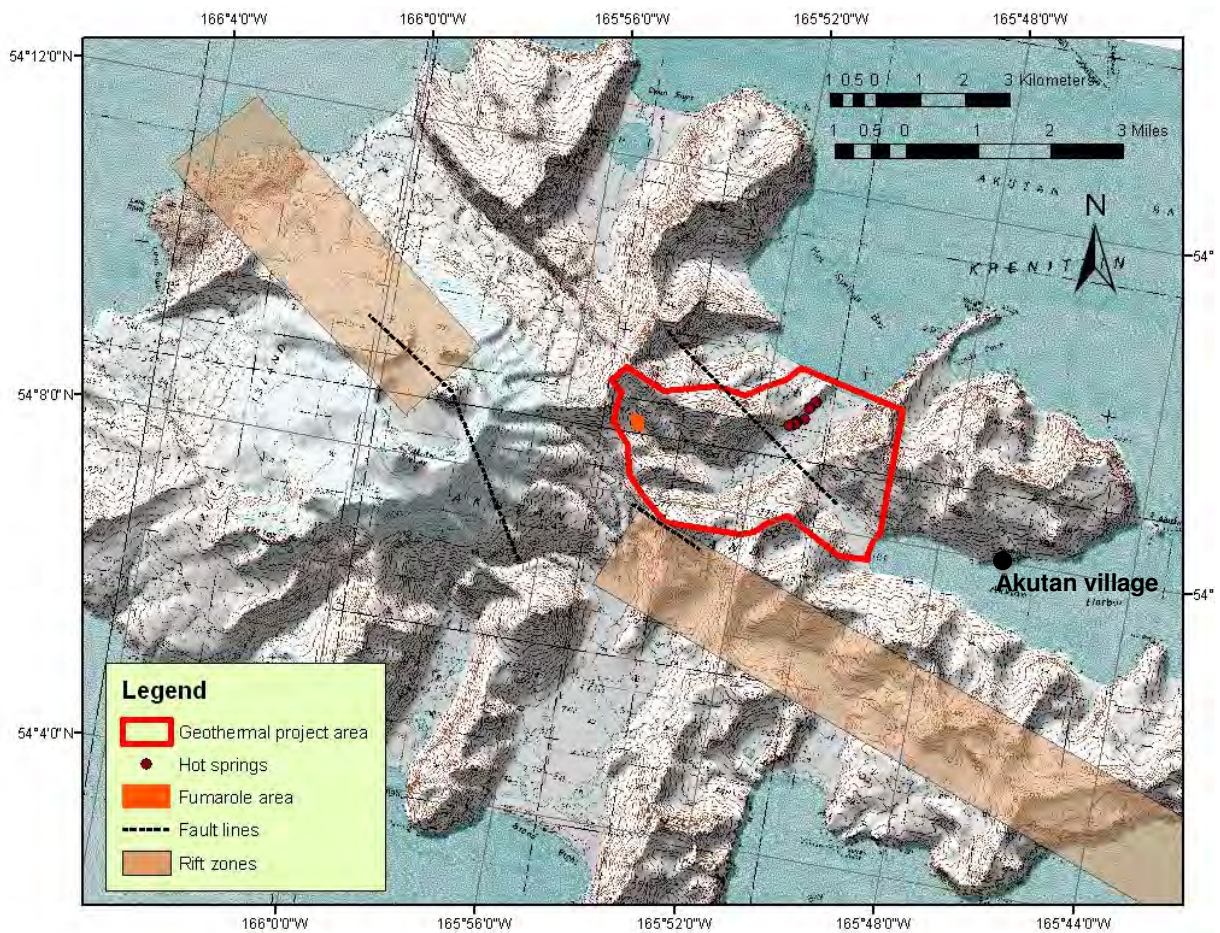
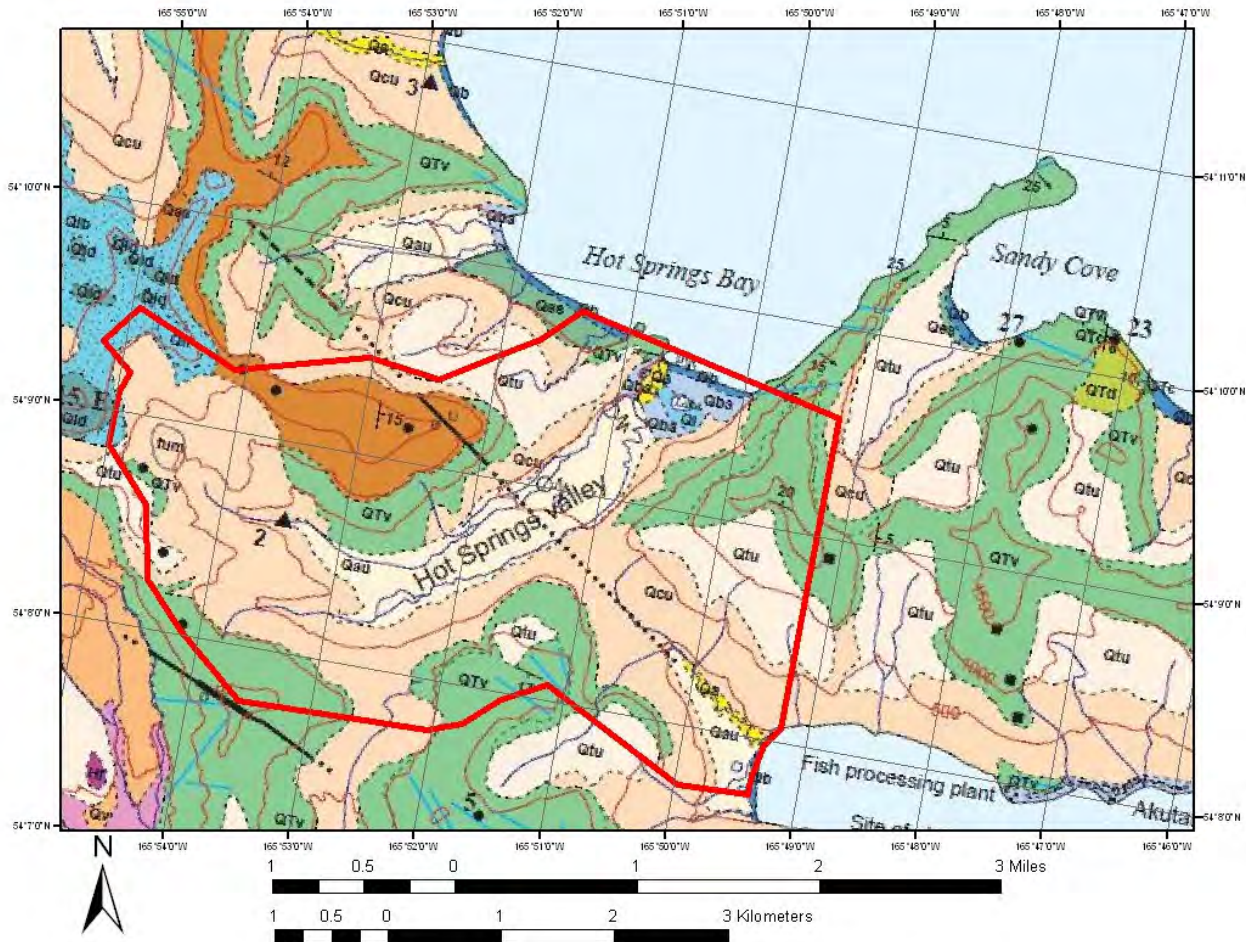


Figure 1. Map of Akutan Island, showing the geothermal area and pertinent geologic features. Faults and rift zones are identified from seismic data (J. Power, pers. comm.)

## Akutan Geothermal Project: Report on 2009 Exploration Activities

A geologic map of the island was published in 1998 by Richter et al. (Fig. 2). The map shows the bulk of the island being comprised of undifferentiated Quaternary/Tertiary volcanic deposits. Hot Springs Bay Valley is one of many glacial valleys that radiate outward from the island's highest point (the volcanic summit).



### Description of Map Units

(See accompanying pamphlet for more detailed descriptions of map units)

#### SURFICIAL DEPOSITS

<ul style="list-style-type: none"> <li><span style="display: inline-block; width: 15px; height: 10px; background-color: yellow; border: 1px solid black; margin-right: 5px;"></span> Q<sub>ax</sub> Alluvium in active stream channels</li> <li><span style="display: inline-block; width: 15px; height: 10px; background-color: lightyellow; border: 1px solid black; margin-right: 5px;"></span> Q<sub>au</sub> Alluvium, undifferentiated</li> <li><span style="display: inline-block; width: 15px; height: 10px; background-color: lightorange; border: 1px solid black; margin-right: 5px;"></span> Q<sub>ou</sub> Coluvium, undifferentiated</li> <li><span style="display: inline-block; width: 15px; height: 10px; background-color: lightblue; border: 1px solid black; margin-right: 5px;"></span> Q<sub>l</sub> Lacustrine deposits</li> </ul>	<ul style="list-style-type: none"> <li><span style="display: inline-block; width: 15px; height: 10px; background-color: lightgreen; border: 1px solid black; margin-right: 5px;"></span> Q<sub>ec</sub> Eolian deposits</li> <li><span style="display: inline-block; width: 15px; height: 10px; background-color: lightblue; border: 1px solid black; margin-right: 5px;"></span> Q<sub>mb</sub> Modern beach deposits</li> <li><span style="display: inline-block; width: 15px; height: 10px; background-color: lightblue; border: 1px solid black; margin-right: 5px;"></span> Q<sub>ab</sub> Abandoned beach deposits</li> </ul>
---	---

#### DEPOSITS OF AKUTAN AND ANCESTRAL AKUTAN VOLCANO

<ul style="list-style-type: none"> <li><span style="display: inline-block; width: 15px; height: 10px; background-color: orange; border: 1px solid black; margin-right: 5px;"></span> 1978 1978 lava flow</li> <li><span style="display: inline-block; width: 15px; height: 10px; background-color: orange; border: 1px solid black; margin-right: 5px;"></span> 1949-48 1949-48 lava flow (shown in cross section only)</li> <li><span style="display: inline-block; width: 15px; height: 10px; background-color: orange; border: 1px solid black; margin-right: 5px;"></span> 1929 1929 lava flow</li> <li><span style="display: inline-block; width: 15px; height: 10px; background-color: orange; border: 1px solid black; margin-right: 5px;"></span> H<sub>0</sub> Modern cinder cone</li> <li><span style="display: inline-block; width: 15px; height: 10px; background-color: orange; border: 1px solid black; margin-right: 5px;"></span> H<sub>1</sub> Younger Sea Lion Rocks lava flow</li> <li><span style="display: inline-block; width: 15px; height: 10px; background-color: orange; border: 1px solid black; margin-right: 5px;"></span> H<sub>2</sub> Older Sea Lion Rocks lava flow</li> <li><span style="display: inline-block; width: 15px; height: 10px; background-color: purple; border: 1px solid black; margin-right: 5px;"></span> H<sub>3</sub> Holocene lava flows</li> <li><span style="display: inline-block; width: 15px; height: 10px; background-color: purple; border: 1px solid black; margin-right: 5px;"></span> G<sub>v</sub> Volcaniclastic deposits</li> <li><span style="display: inline-block; width: 15px; height: 10px; background-color: purple; border: 1px solid black; margin-right: 5px;"></span> G<sub>r</sub> Lahar runout deposits</li> <li><span style="display: inline-block; width: 15px; height: 10px; background-color: purple; border: 1px solid black; margin-right: 5px;"></span> G<sub>ur</sub> Reworked lahar deposits</li> </ul>	<ul style="list-style-type: none"> <li><span style="display: inline-block; width: 15px; height: 10px; background-color: lightgrey; border: 1px solid black; margin-right: 5px;"></span> Q<sub>tu</sub> Tephra</li> <li><span style="display: inline-block; width: 15px; height: 10px; background-color: yellow; border: 1px solid black; margin-right: 5px;"></span> Q<sub>w</sub> Present caldera wall rocks</li> <li><span style="display: inline-block; width: 15px; height: 10px; background-color: lightgrey; border: 1px solid black; margin-right: 5px;"></span> Q<sub>oc</sub> Older caldera (?) plug</li> <li><span style="display: inline-block; width: 15px; height: 10px; background-color: lightgrey; border: 1px solid black; margin-right: 5px;"></span> Q<sub>od</sub> Older caldera (?) dome</li> <li><span style="display: inline-block; width: 15px; height: 10px; background-color: lightgrey; border: 1px solid black; margin-right: 5px;"></span> Q<sub>ou</sub> Older caldera wall rocks, undifferentiated</li> <li><span style="display: inline-block; width: 15px; height: 10px; background-color: lightgrey; border: 1px solid black; margin-right: 5px;"></span> Q<sub>pl</sub> Pre-glacial lava flows</li> <li><span style="display: inline-block; width: 15px; height: 10px; background-color: lightgrey; border: 1px solid black; margin-right: 5px;"></span> A<sub>uv</sub> Ancestral Akutan volcanic rocks, undifferentiated</li> <li><span style="display: inline-block; width: 15px; height: 10px; background-color: lightgrey; border: 1px solid black; margin-right: 5px;"></span> A<sub>co</sub> Ancestral Akutan cinder cone</li> <li><span style="display: inline-block; width: 15px; height: 10px; background-color: lightgrey; border: 1px solid black; margin-right: 5px;"></span> A<sub>pl</sub> Ancestral Akutan plug</li> </ul>
--	--

Figure 2. Akutan geothermal project area (in red) overlaying the geologic map by Richter et al., 1998. "fum" denotes location of flank fumarole area.

### III. Exploration Methods and Results

#### 1. *Geologic reconnaissance and geothermometry*

Results from the 1988 geothermal study were synthesized with the new geologic understanding of Akutan's magmatic plumbing system and with field observations from a 2009 reconnaissance trip to Hot Springs Bay Valley. Field observations were made with particular attention to hydrothermal alteration/deposition patterns, structure, and the permeability of different lithologic units. Updated geothermometry calculations, modeled after Giggenbach (1991), were applied to the 1988 chemical analyses of the Akutan hot springs (spreadsheet models from Powell and Cumming, 2010).

A NW-trending normal fault cuts near-perpendicularly across Hot Springs Bay Valley. This fault, shown in Figs. 1 and 2, is exposed in the lithologic units on both the NW and SE walls of Hot Springs Bay Valley (Fig. 3). Although no trace of the fault is apparent in the valley itself, all of the hot springs occur down-valley from the presumed fault trace, implying structural control.

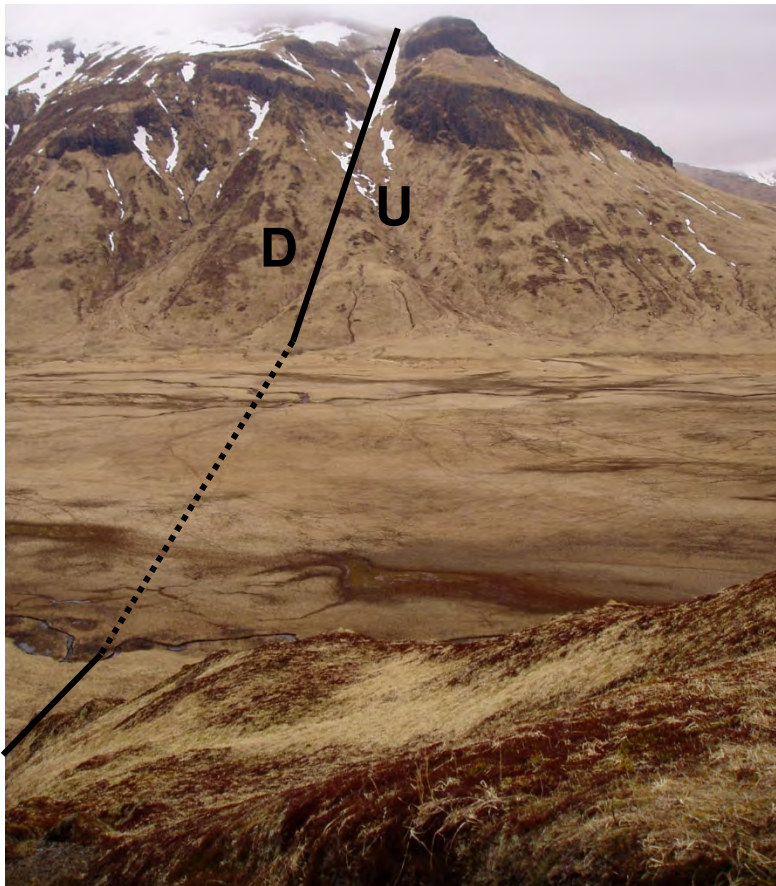


Figure 3. Trace (solid lines) and presumed trace (dashed line) of NW-trending normal fault across Hot Springs Bay Valley.

Hot Springs Bay Valley itself, rather than being controlled strictly by glacial processes as was previously believed (Motyka and Nye, 1988), may be controlled by concealed structure as well. The geomorphology of the NW side of the valley is distinct from that of the SE side of the valley. The NW side is composed primarily of flat-lying lavas, often with pillow morphology (implying a submarine origin) and few dikes. The SE side, by contrast, is rich with dikes and appears to be a subaerial deposit. Thus it is possible that the dike-rich SE wall represents the substrate over which the lavas on the NW side flowed. This dike-rich unit may exist at depth below study area. All of these rocks are from the ancestral volcanic system (see Fig. 2).

Ten separate groups of hot springs were identified, including some tidewater springs on the beach of Hot Springs Bay that are only exposed at low tide. Temperatures ranged from 54-89 °C (130-192 °F). The hottest springs are the furthest upvalley, with temperatures of 89 °C. Though the springs are not associated with any obvious structure, several of them displayed roughly linear orientations perpendicular to the valley but parallel to the NW-trending fault and other lineations (such as the strike of Hot Springs Bay beach). The strike of these lineations was 290°.

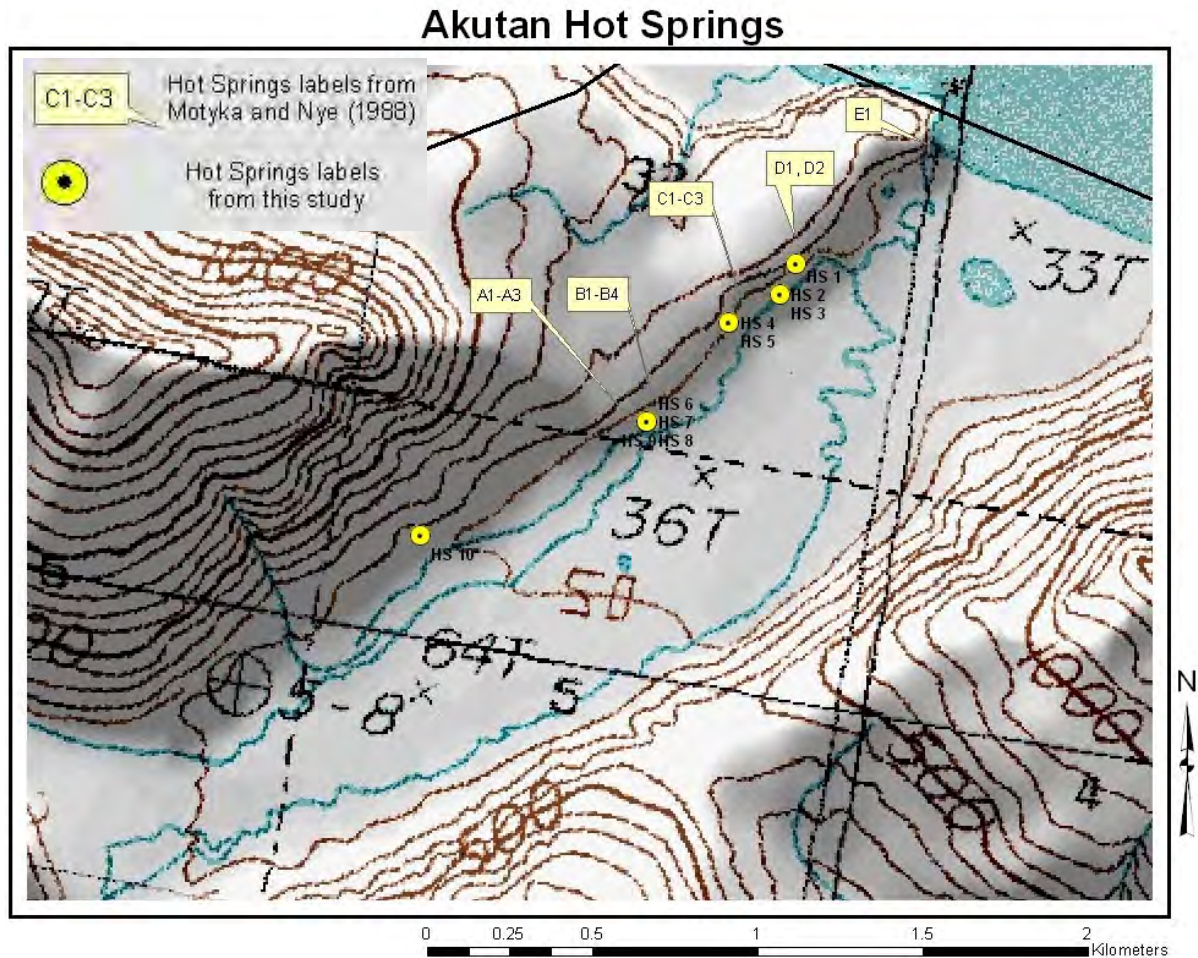


Figure 4. Hot springs locations in Akutan's Hot Springs Bay Valley.

Hydrothermal alteration and deposition in Hot Springs Bay Valley is relatively minimal, occurring only at the hot springs themselves and to a very limited extent. All springs displayed iron (Fe) deposition. A few of the hotter springs had active sinter ( $\text{SiO}_2$ ) deposition (Figs. 5 and 6), commonly indicative of nearby temperatures close to 180 °C.



*Figure 5. Iron (Fe) and sinter ( $\text{SiO}_2$ ) deposition at Akutan Hot Spring group C (see Fig. 4 for spring location).*



*Figure 6. Iron (Fe) and sinter ( $\text{SiO}_2$ ) deposition at Akutan Hot Spring group B (see Fig. 4 for spring location).*

Updated geothermometry calculations (Giggenbach, 1991), were applied to the 1988 chemical analyses of the Akutan hot springs using the Excel liquid chemistry spreadsheets from Powell and Cumming (2010). Table 4 shows values for the common silica (quartz) and cation (Na/K and Na/K/Ca) liquid geothermometers.

Sample	Temp. °C	Quartz Cond.	Na-K-Ca	Na-K-Ca Mg corr	Na/K (Fournier)
Akutan HS A3	84	159	189	169	205
Akutan HS A3	84	155	185	162	198
Akutan HS A3	nd	157	178	162	185
Akutan HS B1	47.4	139	179	138	211
Akutan HS C4	73.4	155	171	137	196
Akutan HS D2	58.8	132	164	11	191
Akutan HS E*	67	148	162	2*	156*

*Table 4. Geothermometer calculations for Akutan hot springs waters. Compositional data from Motyka and Nye, 1988. Computations from spreadsheets presented in Powell and Cumming (2010), based on work by Giggenbach (1991) and Fournier (1989). \*HS E fluids are likely to be mixed with seawater, so geothermometry is probably unreliable.*

The Na-K-Mg ternary plot shown in Fig. 7 gives the sodium-potassium (Na-K) geothermometer along with the potassium-magnesium (K-Mg) geothermometer (after Giggenbach, 1991). This plot suggests that Akutan hot springs waters are poorly to partially equilibrated and/or mixed. Samples B1 and A3 appear to be the closest to partial equilibrium, consistent with their location farthest upvalley. The trend toward 200 or 220 °C is, however, consistent with a higher temperature and more distant source fluid for an aquifer with a nearby temperature >160 °C as suggested by the silica geothermometry and with the sinter found at many of the hot springs.

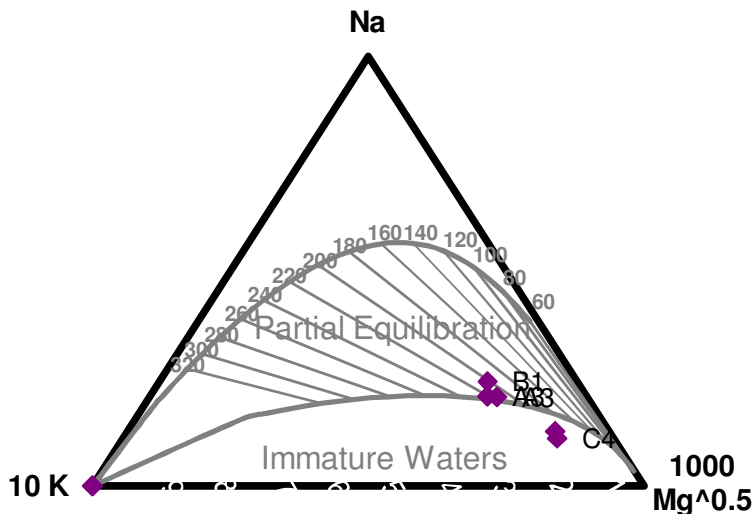


*Figure 7. Ternary plot showing relative concentrations of Na, K, and Mg, and the Na-K and K-Mg geothermometers after Giggenbach (year). Compositional data from Motyka and Nye, 1988. Plot parameters from Powell and Cumming, 2010.*

On the other hand, the fact that Cl is the dominant anion in Akutan hot springs fluids indicates that they arise from a relatively mature hydrothermal system (Figure 8).

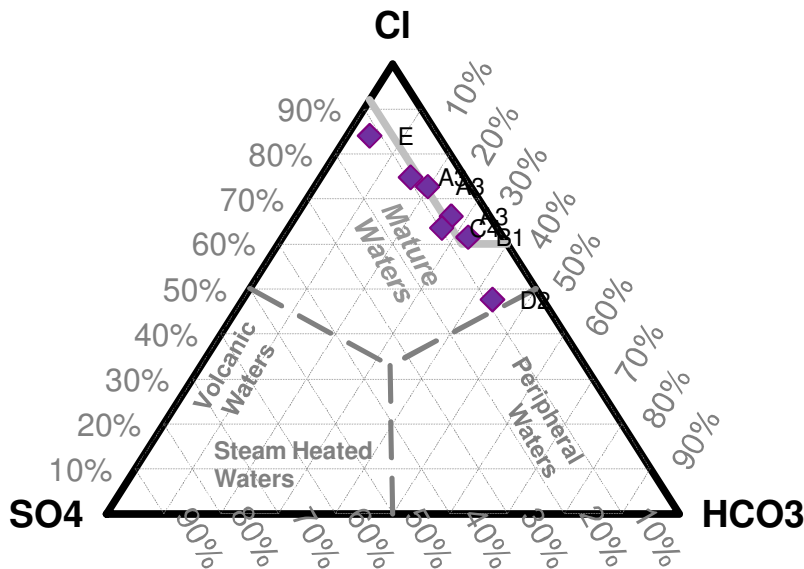


Figure 8. Ternary plot showing relative concentrations of the anions chloride (Cl), sulfate (SO<sub>4</sub>), and bicarbonate (HCO<sub>3</sub>). Compositional data from Motyka and Nye, 1988. Plot parameters from Powell and Cumming, 2010.

Stable isotope data from Akutan hot spring water show that the geothermal fluids are essentially meteoric in origin (Fig. 9).

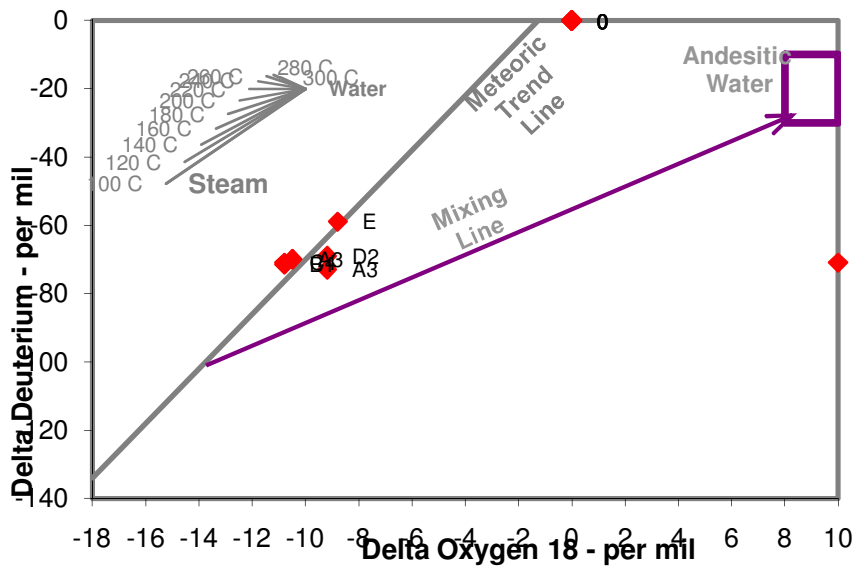


Figure 9. Plot of stable isotope data from Akutan hot springs waters against the meteoric water line. Compositional data from Motyka and Nye, 1988. Plot parameters from Powell and Cumming, 2010.

## 2. Soil geochemical surveys

Mercury (Hg) content in soils can be used as a geothermal resource indicator. Hg is a highly volatile and mobile element that occurs naturally in rocks in very small concentrations. Geothermal heat volatilizes the Hg in rocks and carries it upward and outward from the geothermal source, usually in association with CO<sub>2</sub>. Soil arsenic (As) and Boron (B) are two other geothermal resource indicators. The As and B are carried by geothermal fluids, not gasses, so they are commonly used as a complement to Hg in geothermal exploration studies. All soil and vegetation samples were collected from the Akutan geothermal area with a hand trowel from depths up to 6.” Samples were collected in May and September 2009 and analyzed by ThermoChem, Inc.

Results from the soil and vegetation chemical survey are shown in Fig. 10. Mercury (Hg) anomalies are concentrated near the fumarole field and near the hot springs, which is expected, but also at an unexpected location at the valley ‘elbow’ (that is, where the valley makes a 90° turn to the NE). Arsenic (As) concentrations are highest at the hot springs, also expected since the element is carried by geothermal fluids. Boron (B) concentrations, however, appear to follow the NW-trending fault trace as well as the hot springs outflow pattern. This is an interesting result that could emphasize the importance of the concealed NW-trending fault.

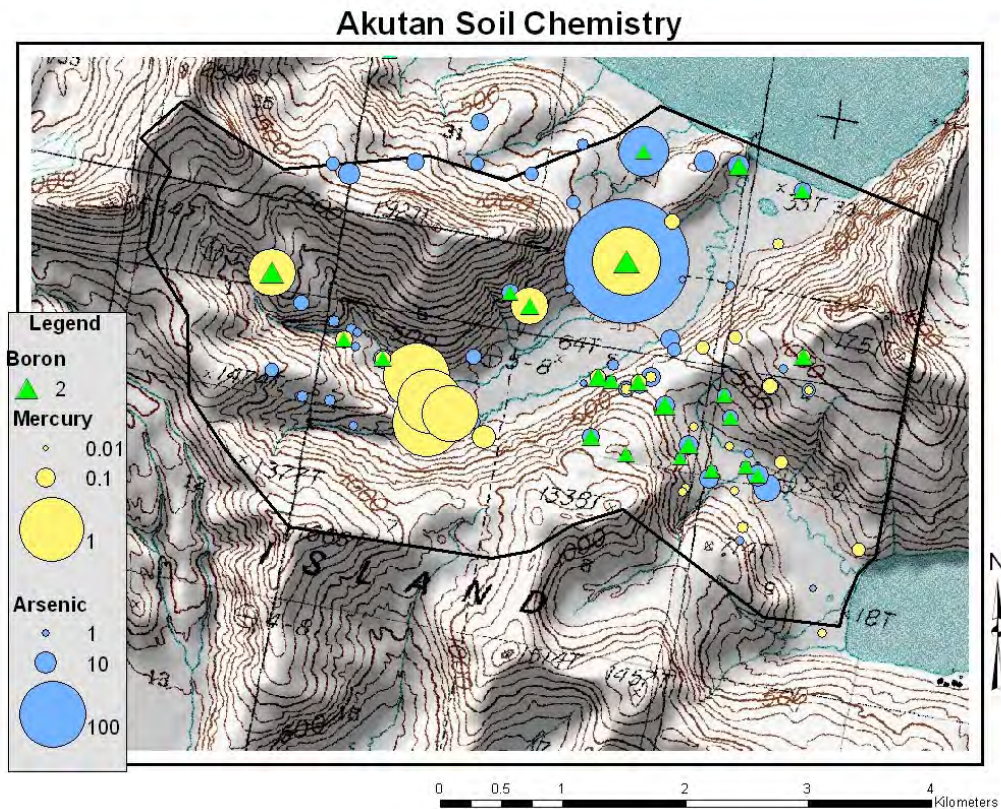


Figure 10. Soil Chemistry results. Note that although Mercury values (yellow) seem to vary by location, the actual concentration in the soil is relatively low (~1ppm). All values in ppm.

Soil geochemistry surveys for the purpose of locating geothermal resources have many limitations. The unique geotechnical properties of Akutan's subsurface (muskeg conditions, poorly documented subsurface microbial processes, complex but poorly mapped structural features, etc.) pose substantial challenges in streamlining sample collection and in interpreting soil geochemical data. Because geothermal volatilization of Hg in rocks usually occurs in association with carbon dioxide (CO<sub>2</sub>), and because CO<sub>2</sub> has also been used as a geothermal tracer, we chose to collect soil gases from sample sites on Akutan as well. Helium was also included in this survey due to its well-documented association with geothermal activity, especially magmatic geothermal activity.

Gas samples were collected Akutan geothermal area using a 3 ft. hand probe, tygon tubing, and evacuated metal cylinders (Fig. 11). All samples were analyzed by ThermoChem, Inc. Gas samples were analyzed for CO<sub>2</sub>, He, Ne, Ar, N<sub>2</sub> and CH<sub>4</sub>; however, this was a package analysis and the elements of interest were CO<sub>2</sub> and He.



*Figure 11. Akutan resident Brett Willis sampling for soil gas on a ridge overlooking Akutan's Hot Springs Bay Valley.*

Results from the soil gas chemical survey are shown in Fig. 12. Helium (He) anomalies occur throughout the geothermal area, which probably reflects magmatic activity in the deep subsurface. The largest CO<sub>2</sub> anomaly is located at the hot springs, but there are several smaller anomalies in the valley 'elbow' and in the NW-trending valley to the SE of Hot Springs Bay Valley. This could reflect structural control on that valley.

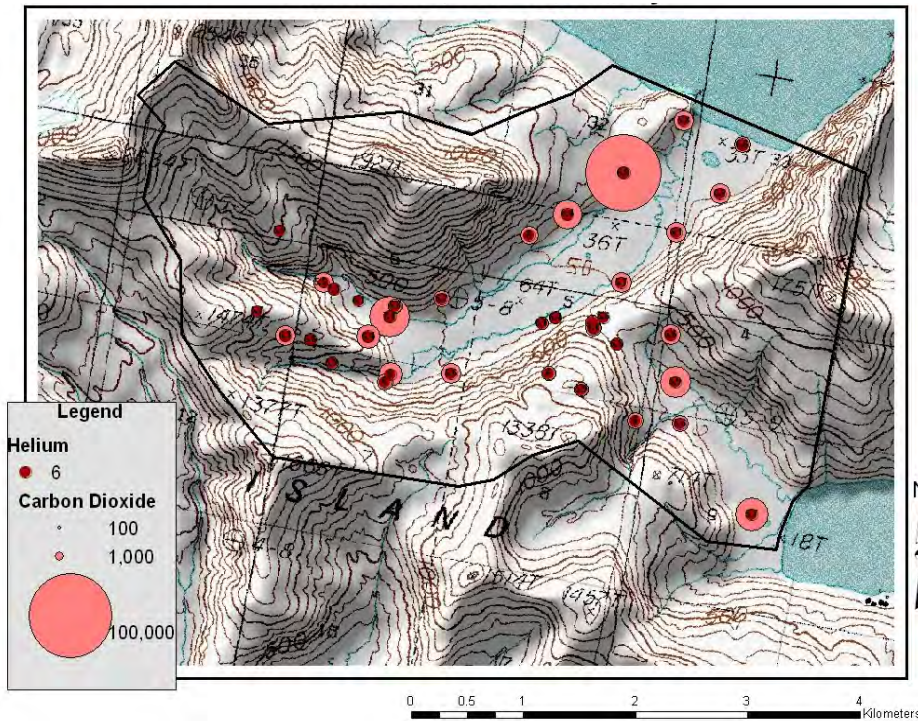


Figure 12. Soil Gas Chemistry results. Numerical values refer to CO<sub>2</sub>. All values in ppm.

Overlaying the most prominent chemical anomalies (CO<sub>2</sub>, Hg, and As) yields interesting patterns (Fig. 13). One pattern could reflect an upflow near the fumaroles field with outflow down Hot Springs Bay Valley. The second pattern could be interpreted to reflect a NW-trending structure that is offset left-laterally across Hot Springs Bay Valley.

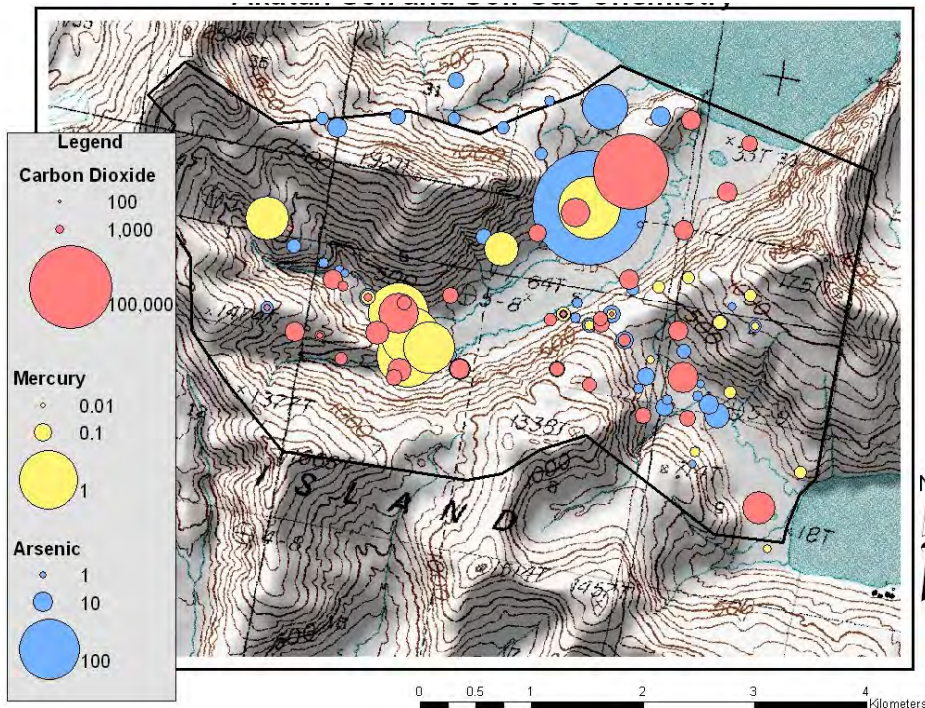


Figure 13. Selected soil and soil gas chemistry results. All values in ppm.

### 3. *Remote sensing*

A reconnaissance level thermal mapping study, using the large archive of available free or low cost satellite images, was carried out for the Akutan geothermal area. The objective of this study was to identify areas of anomalous thermal activity that would serve as targets for field investigation. We used available thermal infrared images from moderate resolution Earth Observing Satellites, such as Landsat and ASTER to generate a thermal anomaly and land surface temperature map of the study area at a regional 1:50,000 scale.

For the Akutan geothermal area we searched the entire archive of Landsat 4, Landsat 5 and Landsat 7 images to find available Landsat imagery. The search resulted in about 190 scenes over the study area. The oldest image was from October 1982 and the most recent image being from June 2009. We went through the quick look of each of the 190 images to identify which ones were potentially cloud-free over the study area. Ultimately, 10 scenes were identified that were snow free and cloud free over the target area of interest.

We first created a spatial subset the entire Landsat scene to extract a smaller scene centered on the Akutan region. We used the same spatial subset on all 10 images. We then extracted a spectral subset from each of the images, pulling out only band/channel 6, which is the thermal infrared channel. The thermal infrared channel on Landsat is a single broad spectral band, spanning a wavelength range of 10.4 to 12.5 $\mu$ m, which is well suited to map thermal anomalies associate with Earth's land surface temperatures. The spatial resolution of the Thematic Mapper thermal band on Landsat 5 is 120 meters, and that on the Enhanced Thematic Mapper on Landsat 7 is 60 meters. The temperature saturation limit for pixel-integrated temperature for these sensors is about 68 degrees Celsius and the NEAT is about 0.2 degrees.

Of the 10 selected images, 4 were from the more recent acquisitions of Landsat 7, where the thermal infrared channel shows distinct striping due to sensor malfunctioning. Though these datasets are not ideal for processing, they still have some utility in thermal anomaly detection because the missing lines are not always at the same spot during repeat data acquisition over the same area. Therefore, areas that may not be scanned in one pass of the satellite may get scanned in the consecutive passes. The remaining 6 scenes were either from Landsat 5 or from Landsat 7 at the time when the thermal sensor was still functioning well. The 6 scenes are shown in Fig. 14.

At first we carried out a manually controlled classification of the thermal gray scale image dividing the image into discrete temperature classes based on thresholds selected by trial-and-error. This simple processing, also known as density-slicing and color coding, gave reasonable results and a first order interpretation on where to focus for detail analysis. We then carried out a high pass filtering on the thermal infrared images to enhance the high frequency variations, which reflect areas of sudden changes in temperature values. The filtered product helped to identify the nucleus or the central point of interest for thermal anomaly detection.

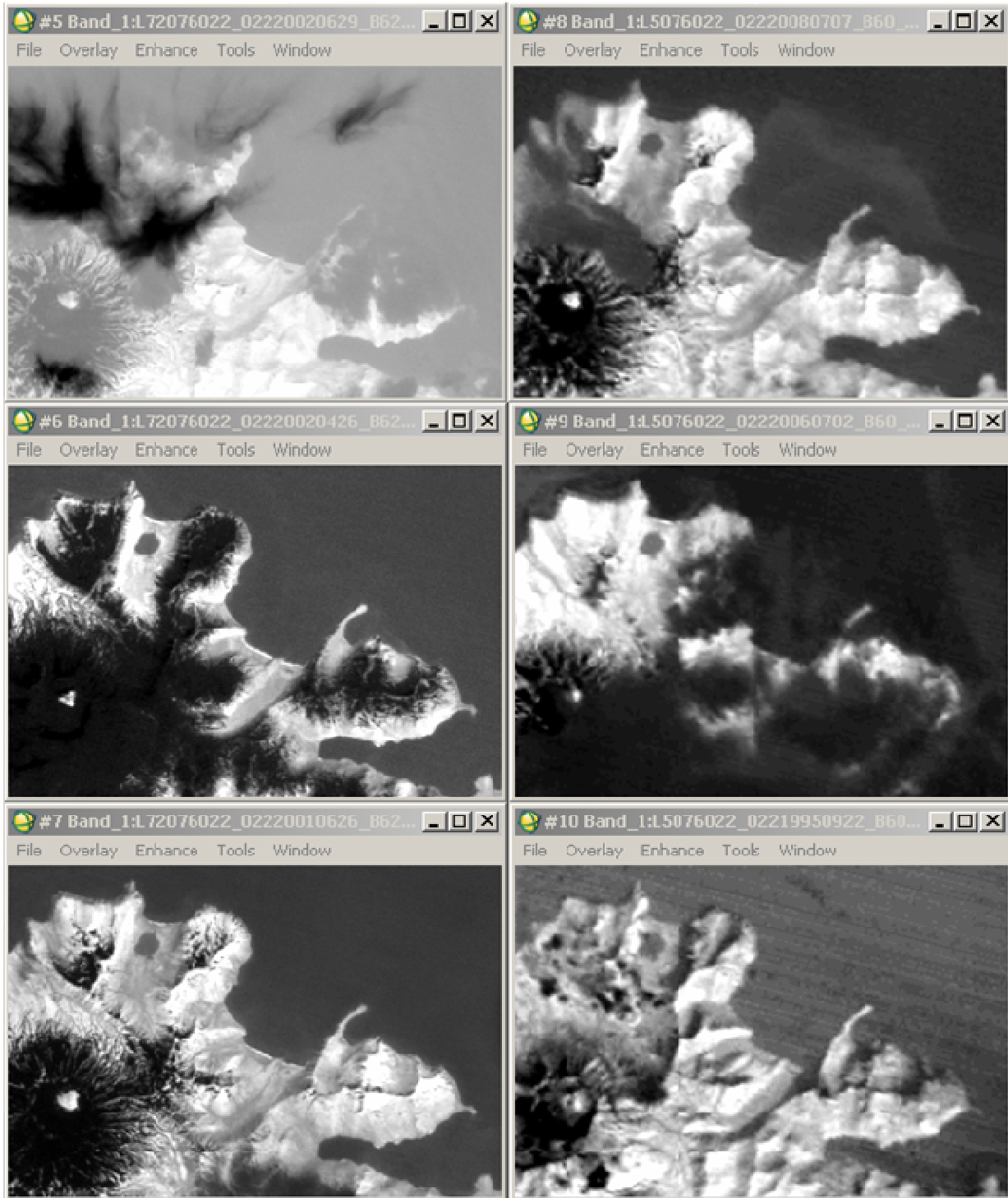


*Figure 14. Six relatively snow free and cloud free thermal infrared images of the study area acquired by Landsat 5 and 7 thermal infrared sensors. Brighter tones depict warmer surfaces and lighter tones depict relatively cooler surfaces. The edifice of the Akutan volcano is clearly visible as a bright spot on the middle left of the images.*

The six scenes shown in Fig. 14 gave a sense of the regional thermal setting of the area. The hot crater of the Akutan volcano, the land water interface, and the geomorphological controls causing differential solar heating in the area clearly stood out. Hilly areas were particularly affected as the south facing slopes showed up brighter (higher surface temperatures) than the north facing slopes. The valley area, which is mapped as thermally active and containing several hot springs, showed up on most of these images in a relatively monotonous gray tone, implying minimal visible thermal contrast, either due to the coarse spatial scale of the satellite image, or due to the surface thermal signature being marred by the alluvial/surficial soil cover and tundra tussock vegetation in the valley area, or due to all the above reasons.

Results of the density slicing are shown in Fig. 15.

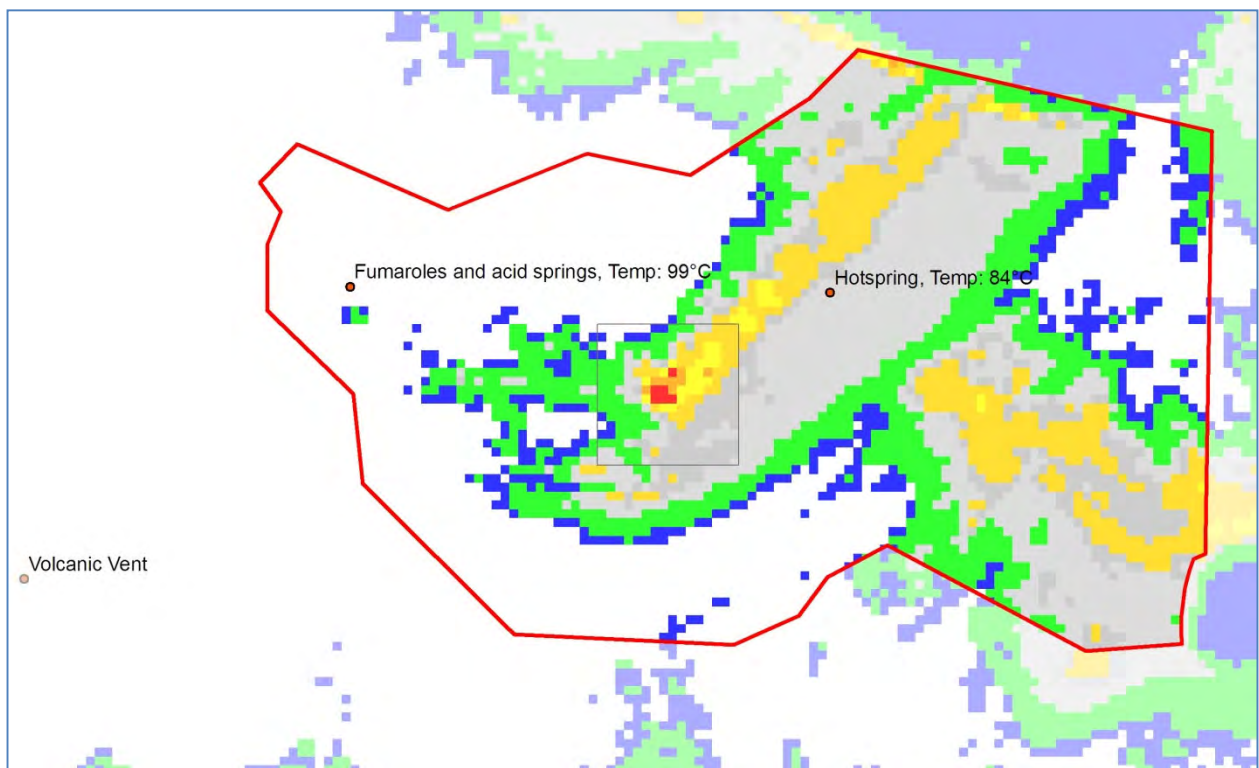


*Figure 15. Density-sliced color-coded Landsat Thermal Infrared Image. Gold, yellow, orange and red denote successively warmer temperatures in the area. Grey tones denote moderate temperatures associated with valley regions. Green and blue tones correlate largely with lower temperatures associated primarily with wet coastal areas and water bodies, respectively.*

Using the combined information from the density sliced-color coded image and the filtered image as input, we selected every point that showed a nucleus of high frequency variation, and isolated at least a 900 meter by 900meter window around it. These small windows were extracted from all 6 thermal images of different dates available the area. The advantage of extracting such localized small windows was that they restricted each subset to a single lithological, geomorphological and topographic class, which was important to exclude any error arising due to either differential heating or emissivity variations amongst adjacent land cover classes.

The 900 \* 900 meter windows were then stacked (overlaid) and their digital values were summed and averaged. This mathematical operation on the image stacked helped to further enhance the actual thermal anomaly from the background area. Two areas that consistently showed up as anomalous on the six image layer stack are shown in Fig. 16. Incidentally, these two areas have not been reported to have any unusual thermal activity in the past reports, and therefore, make interesting targets for further investigation. These areas were the basis for further field tests.

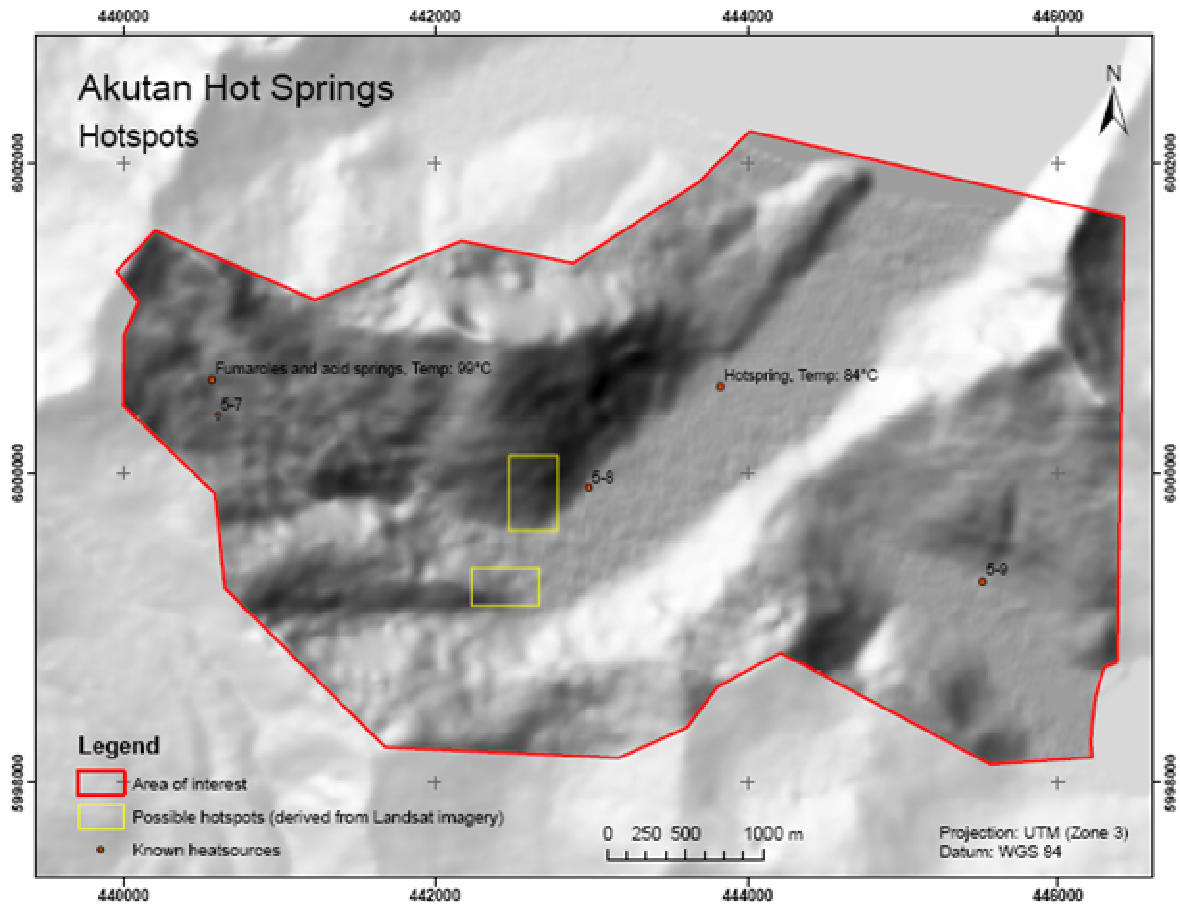


Figure 16. Two areas that consistently showed a warmer surface acquired by Landsat 5 and 7 thermal signature compared to the background on all six thermal images from Landsat are shown in yellow rectangles on this map.

#### 4. MT survey

In August and September 2009, an eight person field crew from WesternGeco-Schlumberger, conducted a resistivity sounding survey at 52 sites in the project area using the magnetotelluric (MT) method.

To detect the resistance to electricity flow in rocks at great depth, the MT method takes advantage of the powerful, naturally occurring electromagnetic waves caused by distant lightening and charged particles from sunspots. In space or in air, the electric and magnetic fields in these waves are consistently coupled but, when they encounter the earth, the electric field causes current to flow in rocks and the electric field dissipates whereas the magnetic field changes comparatively little. The ratio of the electric to the magnetic field provides a measure of the resistance of a rock to electricity flow. Because the electric field of the higher frequency electromagnetic waves dissipates at shallower depth than the electric field of lower frequency waves, MT can be used to detect vertical variations in resistivity by recording a range of frequencies.

Although resistivity is affected by porosity, fluid content and salinity, in geothermal areas, the overall pattern of resistivity is typically dominated by the distribution hydrothermal smectite clay alteration. Gas and fluid from a geothermal reservoir alters overlying and adjacent rocks to smectite clay, which is impermeable to water and has very low resistivity, resulting in the low resistivity clay cap over most geothermal reservoirs. High resistivity is less diagnostic. Although a high temperature, high permeability geothermal reservoir is likely to be much higher in resistivity than the overlying smectite clay cap, very permeable surface lavas that are conduits for cold water are also likely to be resistive. The ambiguous high resistivity zones are interpreted in the context of their geological and geochemical setting.

At Akutan, electrodes were installed at all MT stations to measure electric field but the much heavier magnetometers were installed at only about a third of the MT stations. In areas with difficult access like Akutan, this is a commonly used strategy that works because magnetic field usually varies much more slowly than the electric field. In order to collect sufficient data to overcome noise, mainly due to wind and animals at Akutan, each system collected data overnight and was moved to a new location the following day. There were usually five MT stations running at any given time. Wind noise was a significant issue throughout the survey but, on most stations, it only significantly affected frequencies corresponding to depths much greater than any exploitable geothermal reservoir. However, on one day, strong winds and weak natural signal caused such severe noise that all five recordings were later repeated. With repeats, the 52-station survey took three weeks to complete. A map of the station locations is presented in Fig. 17.

Initial MT processing of the electric and magnetic fields recorded at the station produces an “apparent” resistivity parameter for a range of frequencies. A process called inversion is used to convert this into the true resistivity of a rock over a range of depths below a station. Two MT inversion methods were used to generate map and cross-section displays of the resistivity pattern. Most of the interpretation was done based on a 3D inversion that considered all of the MT data simultaneously and produced a three dimensional mesh of resistivity values beneath Akutan. A simpler 1D method did not reliably resolve resistivity below 1000 m depth but can sometimes produce more reliable resistivity images at depths shallower than a few hundred meters (Cumming and Mackie, 2010).

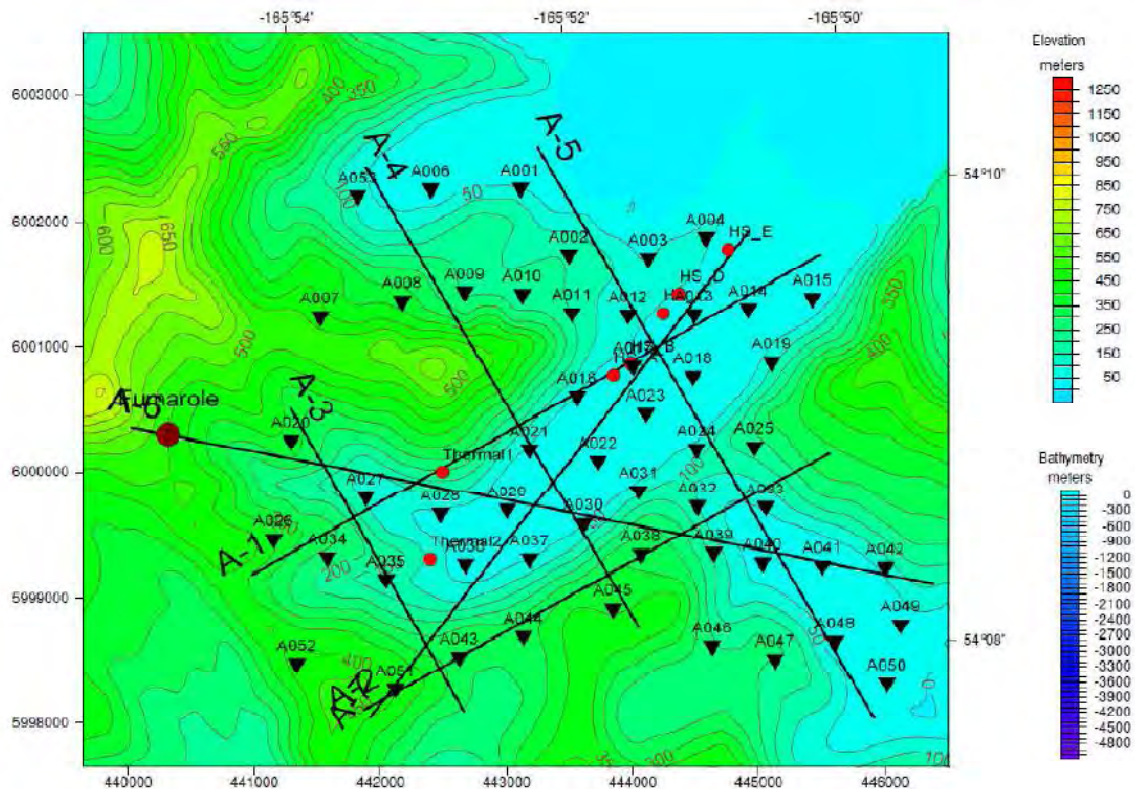


Figure 17. Map of MT stations acquired in August and September, 2009. Triangles represent station locations, red circles indicate the locations of hot springs, and the dark red circle indicates the location of the fumarole area. The two small red circles labeled “Thermal1” and “Thermal2” represent the geographic center of thermal anomalies identified through thermal infra-red remote sensing surveys. The black lines (A-1 – A-7) indicate vertical profile lines.

The MT results are illustrated by 3D and 1D cross-sections included in earlier reports by WesternGeco (2009) and Cumming (2009). The 3D images are emphasized in the interpretation. However, all of the 3D images were compared to 1D images at depths shallower than 1000 m to assess uncertainty. One representative MT resistivity cross-section and one map are included in this report to illustrate how the conceptual models are constrained by the resistivity patterns.

The cross-section and the map reveal a resistivity pattern with a geometry typical of the hydrothermal clay cap that "traps" most economically viable geothermal reservoirs. Figure 18 is a 3D cross section along Hot Springs Bay Valley, following the northwestern valley wall. The green-yellow-red shading represents lower resistivity, generally corresponding to impermeable hydrothermal smectite clay alteration or clay-rich alluvium. The blue shading marks areas of higher resistivity, generally indicating low smectite clay content and, in this context, potentially high permeability. The Akutan fumarole could be projected from about 1 km northwest of this line to a location near station A026. The blue high resistivity imaged below -600 m elevation might correspond to a permeable reservoir zone at >220 °C. High resistivity at the surface usually

corresponds to unaltered volcanics that are permeable but saturated with cold water or air. In the Hot Springs Bay Valley, the yellow-red shallow low-resistivity layer is thin clay cap overlying the aquifer that supports the hot springs.

If the tongue of high resistivity extending toward the surface below station A07 is realistically imaged, it may imply a local  $<180\text{ }^{\circ}\text{C}$  upflow from a tabular aquifer at  $-350\text{ m}$  elevation to a shallower aquifer at about  $-60\text{ m}$  elevation. The proposed zone of moderate temperature upflow occurs below several hot springs. These features can be seen in the resistivity map shown in Figure 18.

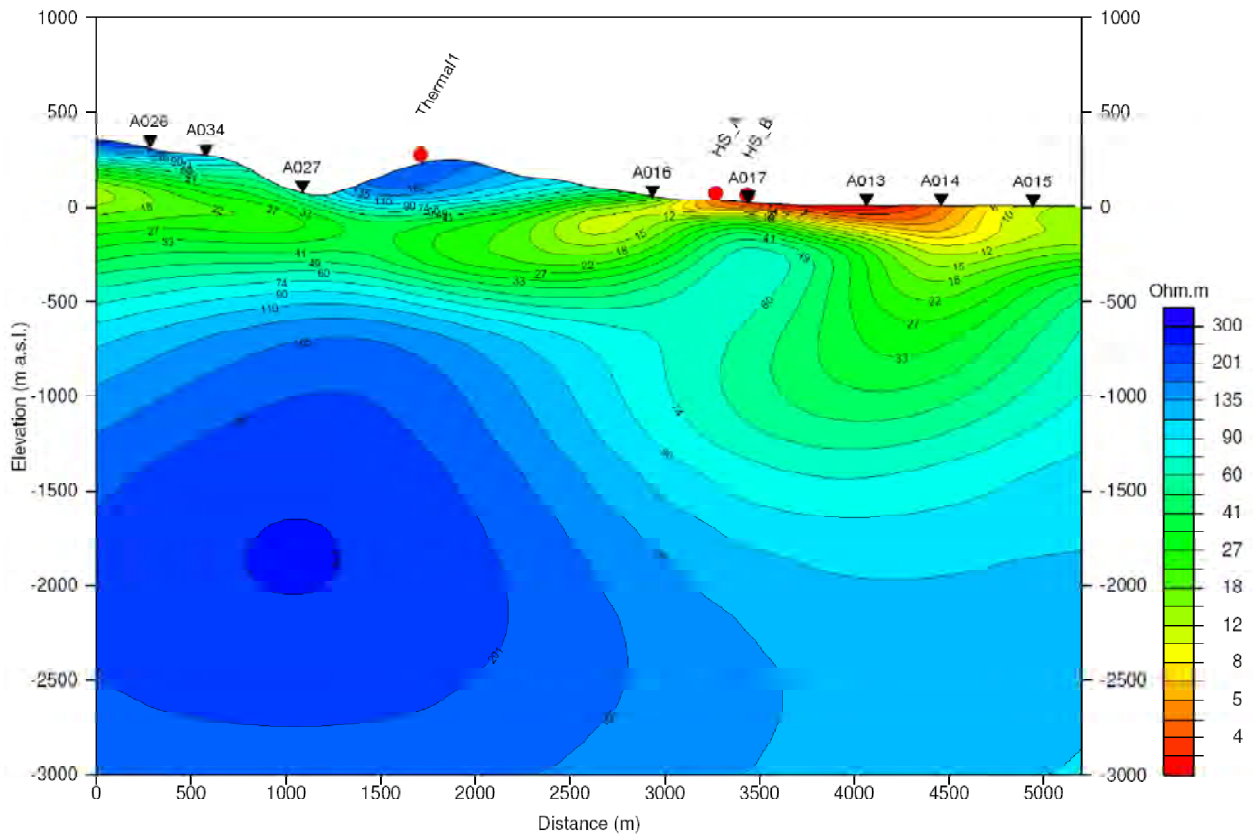


Figure 18. Profile A-1 of electrical resistivity along the length of Hot Springs Bay Valley (see Figure 17 for location).

The map of 3D resistivity at  $-400\text{ m}$  elevation in Figure 19 illustrates similar points to the cross-section. However, it provides a better depiction of the very limited resolution of the likely location of high temperature upflow source of the geothermal system due to the restricted coverage where access and suitable station sites was limited by severe topography. This includes the areas near the fumarole and to the northeast of it. With caveats concerning the uncertainty of the 3D maps in areas with large data gaps, interpretations can be based on the map pattern with reasonable confidence because they are consistent with what would be expected based on geochemistry and other data sets.

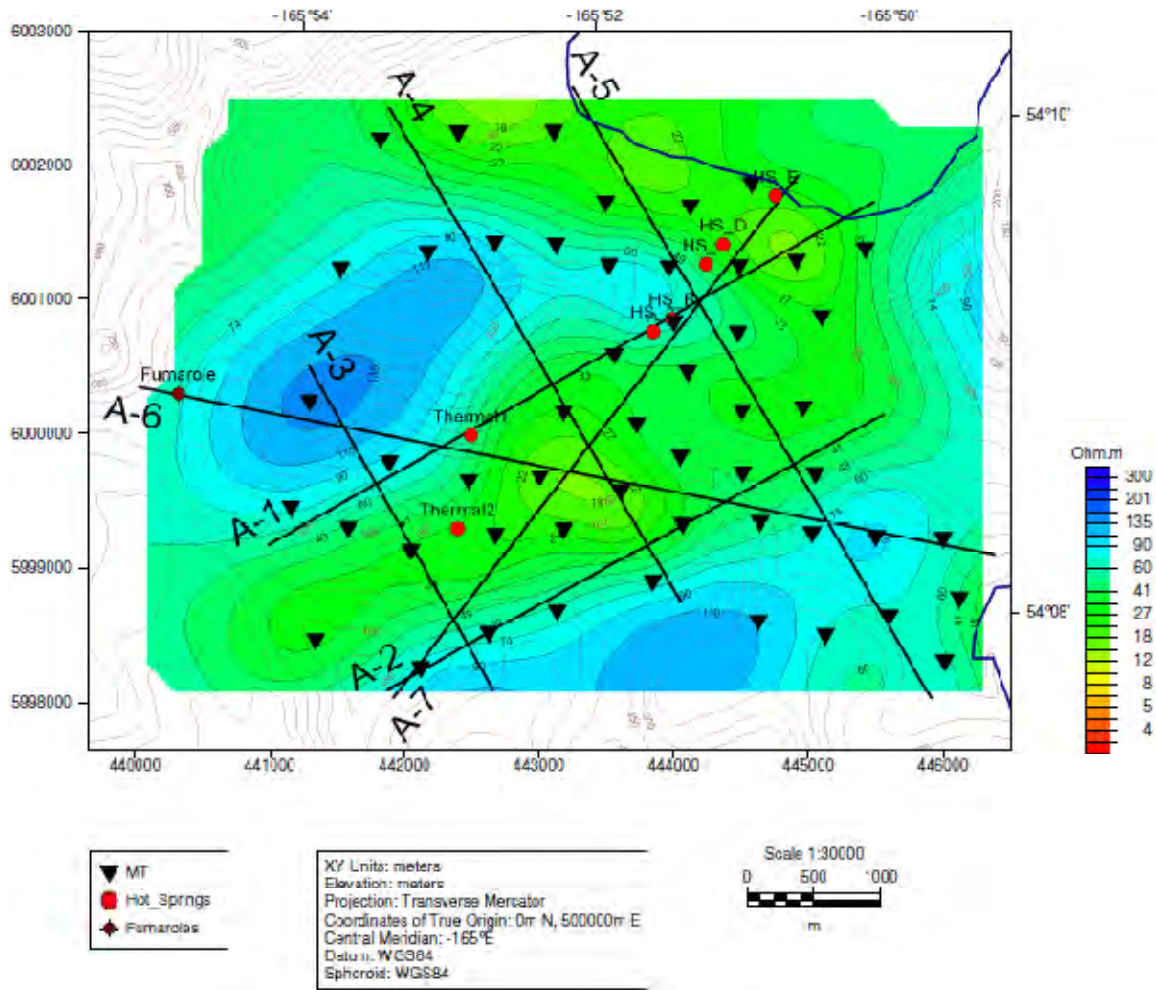


Figure 19. Example of a 3D inversion of MT data, here showing resistivity at -400 m. For additional depth-slices see Hallinan (2009).

The 3D MT resistivity maps at -500 m, -400 m and -300 m elevation are fairly consistent and so only the resistivity at -400 m elevation is shown (Fig. 19). The highest resistivity is at station A020, the station closest to the fumarole. The trend of the high resistivity connects the area near the fumarole to a zone between stations A012 to A016, centered on station A017 near hot spring B. This is consistent with a high temperature zone below the fumarole extending in a shallow outflow to the hot springs. Deeper resistivity maps at -750 and -1000 m elevation show a similar pattern but extending farther north. The accessible location closest to high resistivity areas at -400 m and -1000 m is probably in the fumarole valley, near MT station A027 (station locations shown in Fig. 17).

The resistivity pattern beneath the Hot Spring Bay Valley is consistent with a shallow low resistivity cap over a shallow and relatively thin boiling point aquifer. The low resistivity alluvial fill in the valley appears to be thinner on the northwest margin and

deeper and thicker on the southeast margin based on the cross-section in both Cumming (2009) and WesternGeco (2009). The clay alteration extends to the east but the overlying volcanic rock that forms the southeast rim edifice appears to be generally resistive, unaltered, and intruded by dikes that appear to be permeable, perhaps promoting influx to the reservoir.

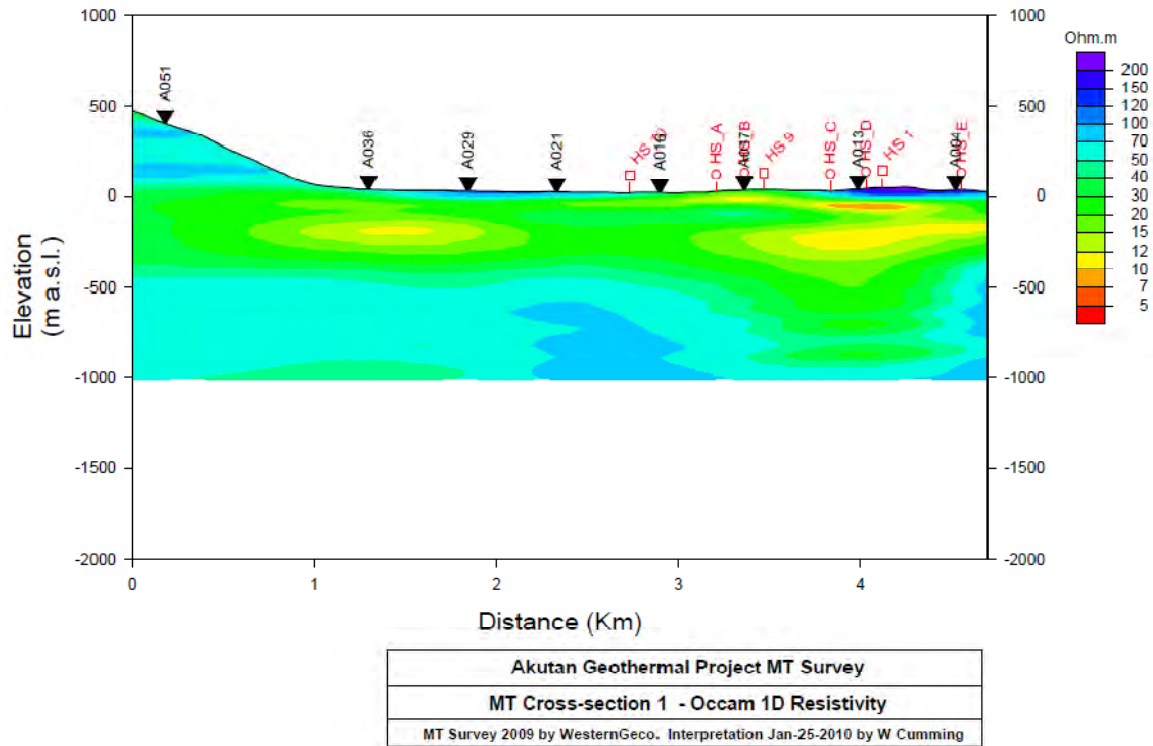


Figure 20. Cross-section B1 is similar to A1 in Figure X but uses 1D MT inversions of particular stations to assess shallow aquifers. A very thin clay cap shallower than 50 m is 5 to 15 ohm-m resistivity, shaded orange to light green. and yellow over an aquifer in green at about 50 m depth. Another zone of high clay extends to 350 m depth.

In Figure 20, MT stations A016, A037 and A013 span the hot springs with the highest geothermometry and measured temperature, A and B. The 1D MT inversion appears to resolve an aquifer at about -20 to -120 m elevation and perhaps below -350 m elevation. This overall geometry is similar to what is resolved by the 3D MT, although the 3D resistivity pattern that hints at deeper upflow is not resolved by the 1D MT inversion.

At depths shallower than 400 m near the hot springs, the 1D MT inversion seem to better resolve a very shallow aquifer and overlying and underlying impermeable clay zones. The 3D inversion appears to resolve a possible break in the deeper clay zone and perhaps an upflow from deeper to shallower tabular aquifers.

## 5. *Thermal field mapping*

Ground soil and surface temperatures were measured at 65 locations in and around Hot Springs Bay Valley. Temperature measurements were made at nearly every geophysical station and soil chemistry sample location during the field campaign in August and September of 2009. Special efforts were made to take temperature measurements above observed thermal anomalies identified in satellite imagery, although it proved too difficult to reach the thermal anomaly located on steep terrain. The area above the other thermal anomaly and the region between the two anomalies were heavily sampled in an effort to resolve the extent of thermal signature in the soil.

At each measurement location a handheld K-type thermocouple (Lutron TM-902C; +/- 1°C) was used to measure ambient air and soil temperatures. At ~2/3 of the locations, air temperature measurements were recorded (after the thermocouple had equilibrated; >60 seconds). At all locations, soil temperatures were measured by inserting the 3" (8 cm) probe into the soil at the base of a ~8" (~20 cm) deep hole (typically dug for taking soil samples or deploying electrical coils for the MT survey), such that the tip of the probe was 11" (~28 cm) below the surface at the time of measurement. The thermocouple was allowed to equilibrate for >60 seconds before the temperature was recorded.

Overall, soil temperatures at a depth of approximate 1 ft. appear to be predominantly controlled by solar influence. Soil temperatures did not vary significantly from the air temperature in any region with the exception of measurements made adjacent to two of the hot springs (35 °C and 94 °C). Soil temperatures taken > 20 meters from any active hot spring ranged from 6 – 11 °C, which mirrored the ambient air temperatures. In only one instance (disregarding the hot springs measurements) was the soil temperature more than 1 °C warmer than air, and in two instances the soil was 3 °C colder than the air. The area above and between the thermal anomalies identified in satellite imagery showed no significant increase in soil temperature, air temperature, or deviation between soil and air temperatures. Field calibration of the thermocouples and the detection of thermal anomalies near the hot springs suggest the equipment was working properly.

## Soil Temperature

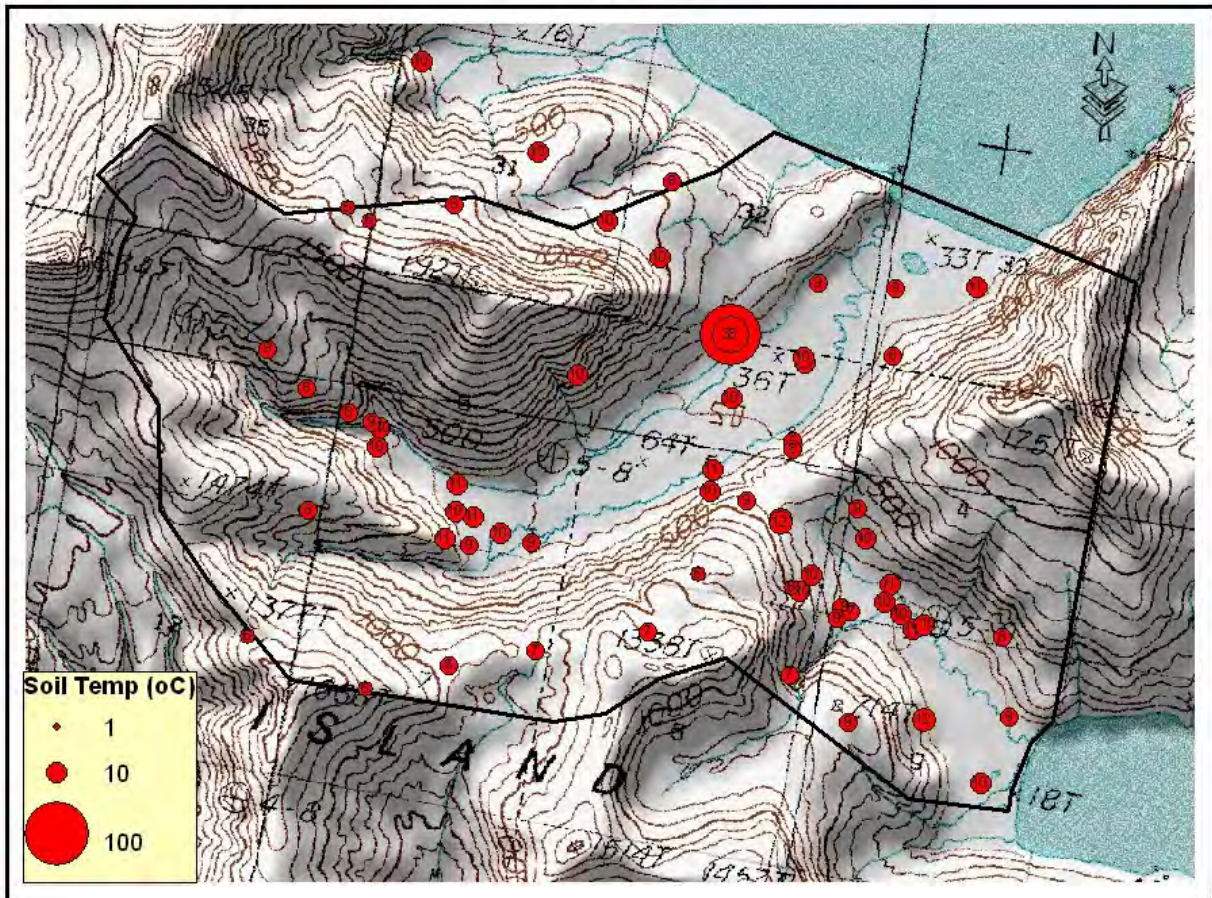


Figure 21. Map of ground temperatures in Akutan geothermal are showing that most of the shallow volcanics are cold, except for elevated temperatures associated with surface alteration around the hot springs.

## IV. Discussion

### 1. *Geothermal resource interpretation*

The composition of Akutan hot springs fluids is unusually dilute relative to other geothermal systems (D. Rohrs, pers. comm.), which could indicate either that they do not originate from a well-equilibrated geothermal reservoir, or that the fluids are mixing with cold groundwater in the subsurface. Such low concentrations could be attributed to significant steam heating of the system, or the waters may be heated conductively by some very young volcanic rocks or dikes.

The disparity between the cation and silica geothermometry implies that the geothermal zone where the geothermal fluids have last equilibrated with the rocks at  $>220$  °C is probably farther than 500 m, perhaps farther than 2000 m, from the hot springs. While the cation geothermometry indicates that a geothermal reservoir of  $>220$  °C probably exists at Akutan, the silica geothermometry of  $\sim 160$  °C indicates that the resource close to the hot springs that is easily accessible ( $<500$  to 1000 m distance and depth) is likely to be 160 to 180 °C.

Due to the frequent eruptions of Akutan volcano, there is likely to be a magmatic vent system and possibly an acid-core zone associated with gas rising from a persistent magma system (e.g. Reyes et al. 1993). However, the neutral cation geochemistry of the hot springs is strong evidence that a neutral system exists. Case-histories suggest that an acid-core zone would isolate itself from a neighboring neutral geothermal system by a 'rind' of impermeable rock, typically created by silica and anhydrite deposition where incompatible acid and neutral fluids interact (Wood, 1994). Conduction through the impermeable rind or above episodic dike intrusions on the flank of Akutan volcano could provide heat for a neutral chloride geothermal convection system adjacent to the active vent system. This is consistent with the rifting model of Lu et al., (2000) who conclude that recent earthquake swarms indicate that Akutan's magmatic system is associated with island-wide extension and subsequent dike emplacement.

It is not clear whether the NW-trending normal fault that cuts at a near-perpendicular angle across Hot Springs Bay (see Fig. 1) is acting as a conduit for geothermal fluids or as a barrier. The fault could be hosting a dike at depth, which could be the heat source for the hydrothermal manifestations in Hot Springs Bay Valley.

According to Motyka and Nye (1988), the Hot Springs Bay Valley is floored by a debris flow which is acting as an impermeable cap over the subsurface hydrothermal system. From very shallow 1988 electrical resistivity and seismic refraction surveys, they interpret this "cap" to be 30-40 m thick. The MT results are consistent with a thin zone containing low resistivity hydrothermal clay acting as a cap over a shallow hot aquifer extending between hot springs groups A and C. The MT also resolves an underlying zone of alteration that thickens to the southeast side of the valley and near the shore. The geothermal manifestations (including ground temperature anomalies) are limited to the

NW side of the Hot Springs Bay Valley, consistent with the clay being very low in resistivity and thin at that margin. Because the low resistivity clay extends across the valley and becomes thicker to the southeast, it is possible that the hot aquifer also extends across the hot springs valley, at greater depth to the southeast. However, hot springs do not appear where the clay is truncated against the very heterogeneous rocks on the southeast margin of the valley.

The fact that the ground temperature survey yielded anomalies only at the hot springs area is neither disappointing nor unexpected. Rather, it is typical of volcanic areas that have unaltered and permeable lavas covering much of the surface and shallow subsurface. In these types of geologic settings, the thermal anomaly is “trapped” beneath the clay cap and therefore temperature gradients begin increasing only below the clay cap. This pattern has been observed at many geothermal areas such as Glass Mountain (NV) and many New Zealand fields.

### **Conceptual Models**

Two conceptual models have been prepared that illustrate median models that could be reached from accessible locations. These also illustrate two drilling targets. The conceptual elements of these models are summarized below.

#### **A magmatic core and/or an acid-core of the volcano**

The frequently erupting volcanic cone implies at least a magmatic throat. Evidence for an acid-core hydrothermal circulation system is more ambiguous. There is a summit lake but its chemistry is unclear. Fumaroles with active sulfur deposition are not mentioned.

#### **Hydrologic barrier between magmatic/acid core and neutral reservoir**

Such barriers are expected due to mineral deposition where chemically incompatible acid and neutral water types mix. Evidence for such a permeability barrier includes the lack of extensive alteration that would be associated with an extensive acid-core. The neutral chemistry of the hot springs and low sulfate suggests little connection to a magmatic or acid core. Neither active native sulfur deposition nor high gas are mentioned at the flank fumarole field.

#### **Neutral chloride upflow at >220 °C**

Although all models have a neutral chloride upflow, its location, lateral size, vertical extent, and temperature vary. The heat source is conduction from the volcano or from deeper dikes under the fumarole area causing convection. A neutral chloride upflow at >270 °C is reasonably likely, located near the fumarole. A modern fumarole gas analysis would be needed to thoroughly assess the likelihood of this. It may extend to the north and east based on interpolated 3D MT imaging. However, a more likely case is the one shown in Figure 23. The size of this zone has very little influence on targeting, except identifying the potential value of both targets at the closest to the kernel of this zone. The volumetrically pessimistic case with a lower confidence level, perhaps 10%, would not have a deep source at 300 °C. A model that might be

typical of a pessimistic resource upflow capacity might have a resource hosted in a low volume, relatively shallow convection cell with a maximum permeable temperature of about 220 °C. Probably only the 160 to 180 °C outflow would be economically developable, if it was thick enough.

### Neutral chloride outflow

This starts somewhere near the fumarole and outflows to and along the valley. In models 1a and b (Figs. 23 and 24), the outflow follows the surface trend of the valley, that is, initially flowing SE and then making an abrupt 90° turn at the ‘elbow’ to the NE. In models 2a and b (Fig. 25 and 26), outflow does not follow any surface morphology but some concealed subsurface structure to flow ENE from the fumarole field towards the NE margin of the valley. In both cases, there appears to be two separate tabular aquifers (or more) in Hot Springs Bay Valley; one at depths of ~100 m and another at depths of ~500 m directly beneath the shallow one. These two aquifers are probably separated by an aquitard of hydrothermal clays and/or glacially deposited clays and tills. The size of the outflow cannot be constrained due to data limitations (from poor access to everywhere beyond the valley floor). However, the minimum size of outflow system appears to be about ~1km long x 500m wide.

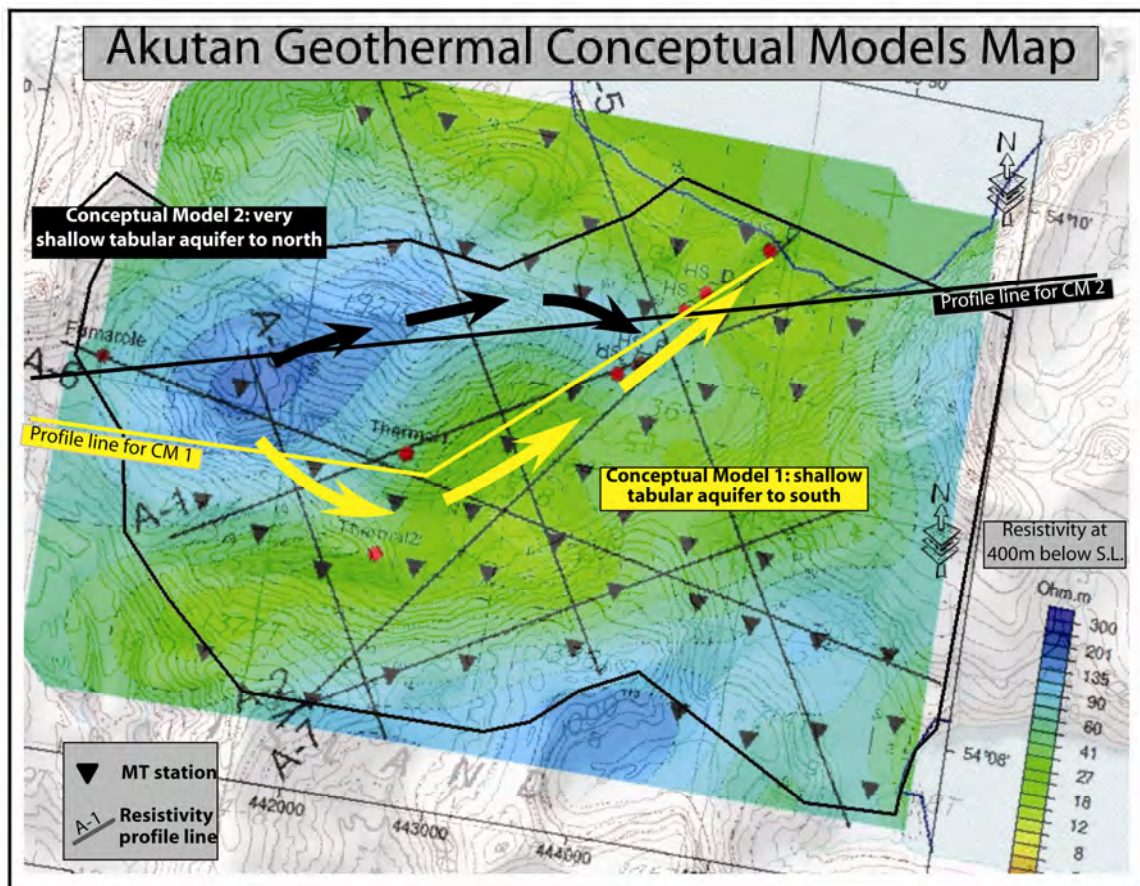


Figure 22. Map showing the two conceptual models for the Akutan geothermal system, overlaid atop a resistivity depth slice at -400 m. The depth slice shows a resistive zone (in blue) interpreted to be the upflow location.

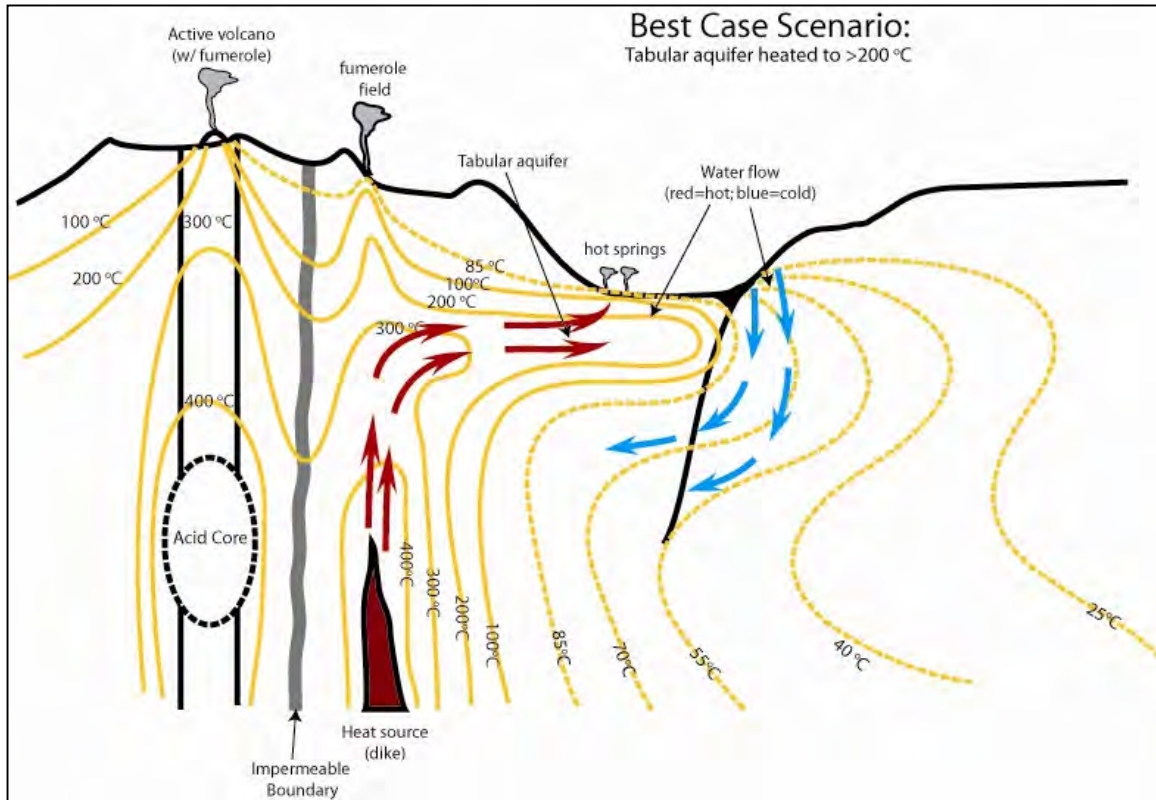


Figure 23. Conceptual model 1a for the Akutan geothermal system.

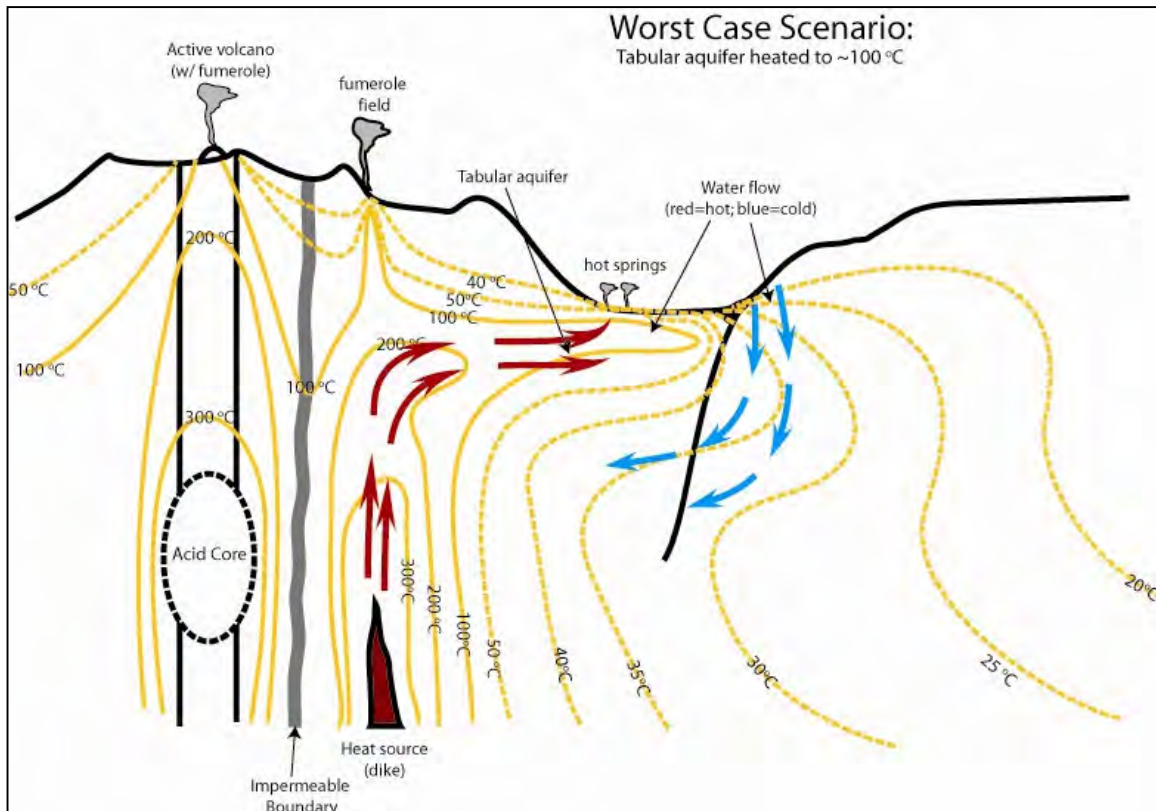


Figure 24. Conceptual model 1b for the Akutan geothermal system.

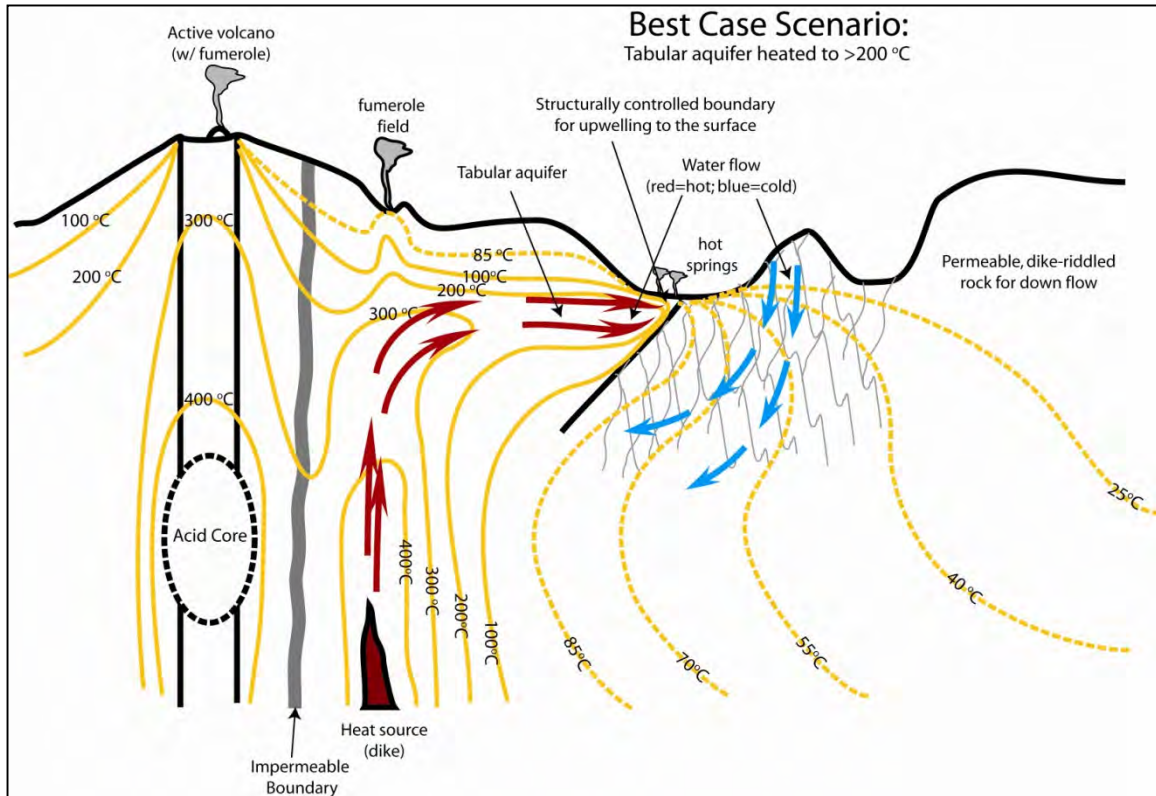


Figure 25. Conceptual model 2a for the Akutan geothermal system.

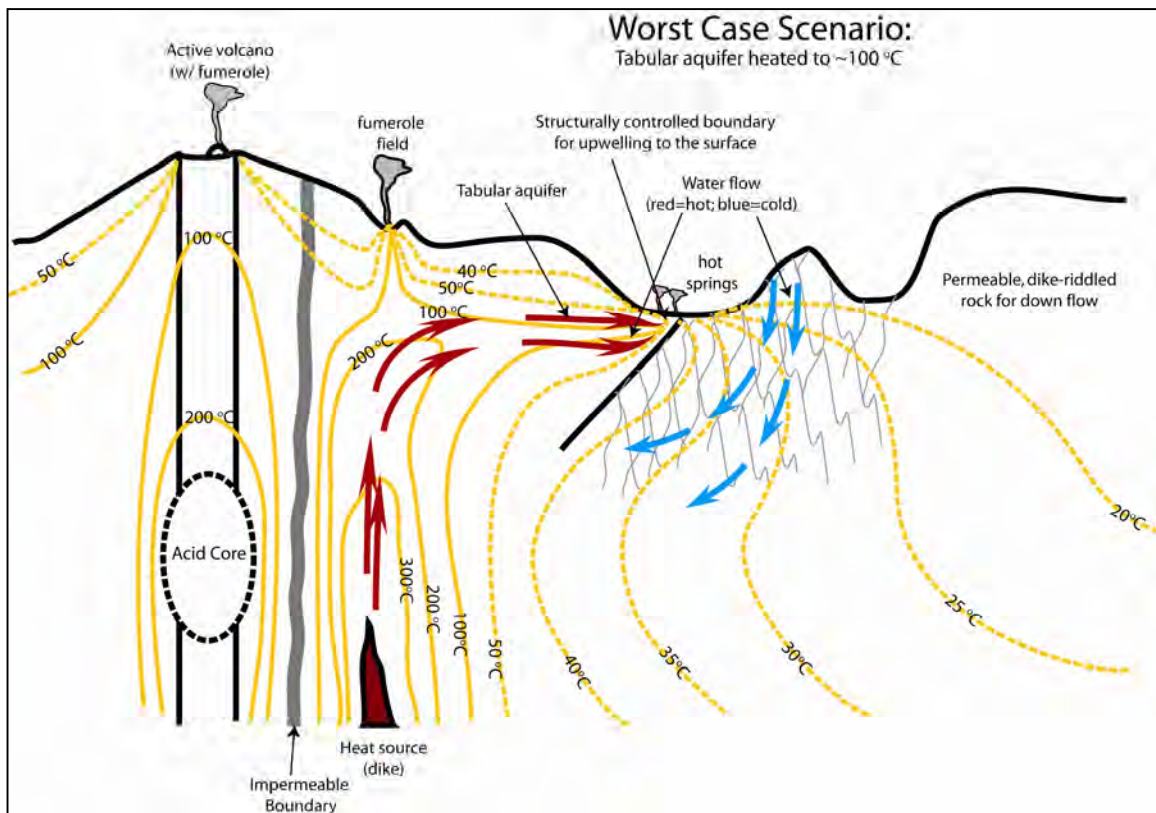


Figure 26. Conceptual model 2b for the Akutan geothermal system.

## 2. *Exploratory well drilling*

Almost all of the exploration data suggests that the likely upwelling location is in the general vicinity of the fumarole field. The MT data, the only dataset that “images” the subsurface, implies that it could be a bit north of this field. However, the fumarole field is located on an extremely steep hillside at about 350 m elevation. This poses severe limitations in terms of access, which are not trivial to the logistics of exploratory drilling and resource development. Hence, drilling targets will have to be a compromise between resource location and accessibility.

Based on the conceptual models of the Akutan geothermal reservoir presented in Figs. 23-26, we propose to drill two to four slimholes at locations given in Fig. 27. These wells will provide temperature gradient measurements in key locations that will determine the viability of geothermal development at Akutan. The well will be designed so that, if a permeable hot aquifer is encountered, it will usually be possible to induce temporary flow so that fluid samples uncontaminated by drilling fluids can be taken for geochemistry analyses. The focus of this will be analyses of the likely temperature of the deep source of the thermal fluids.

Well 1, located in fumarole valley at the bottom of the hill beneath the fumarole field will be drilled to a TVD of 1500 m (3500 ft.). This is the highest priority well as it is believed to be closest to the high temperature upflow zone for the geothermal fluid, although probably on the margin of this zone. If this well encounters >250 °C and evidence of permeability, the likelihood of generating >20 MW with a minimum number of wells would be higher. Follow-up full sized wells could be drilled directionally to the east or northeast.

Well 2, near hot springs group A, will be drilled to 500 m (1500 ft.). This well is the next highest priority. The site appears to be located where a 160 to 180 °C tabular outflow from the higher temperature upflow located to the southwest intersects Hot Springs Valley. The geophysics suggests that two tabular aquifers could be penetrated at relatively shallow depths. This well will be drilled in stages designed to make induced flow from the aquifers feasible, in order to provide geochemistry constraints of the aquifer and deeper system.

Wells 3 and 4 will also be drilled to 500 m (1500 ft.). They are targeted on the outflow zone and will provide constraints on the geometry, temperature variations, and flow patterns of the outflow. These wells, drilled at the junction of the two valleys, will also elucidate which of the conceptual models (Figs. 22-26) is most accurate.

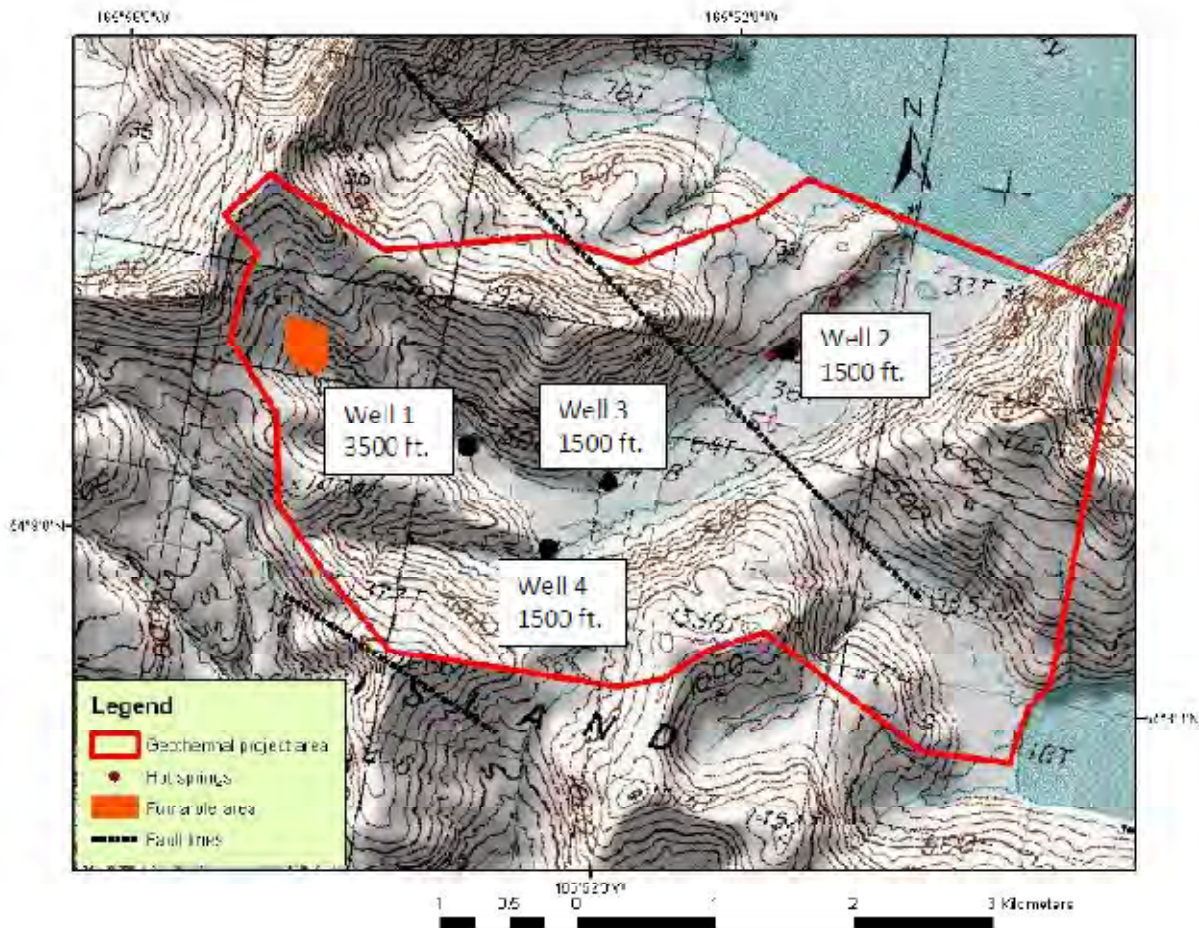


Figure 27. Drilling locations and proposed depths for Akutan exploratory geothermal drilling program.

### 3. Geothermal development

The feasibility of geothermal development at Akutan, and the type of development, is entirely dependent on the results of the exploratory drilling program. Exploratory drilling will provide concrete resource parameters, including:

- Geothermal fluid temperature
- Geothermal fluid flow rate / reservoir pressure
- Geothermal fluid and gas composition
- Cooling temperature (air or cold water sink)
- Location of geothermal production wells

In the worst case scenario, the shallow outflow zone (see Figs 23-26) is the only accessible resource. In that case, the developable capacity is probably less than ~1MW. In another case, the deeper aquifer underneath the shallow one (see Figs. 23-26 and 20) is accessible. In that case, the aquifer could yield up to 10 MW but probably no more as it is

still an outflow feature. In the best case scenario, production wells could be drilled immediately adjacent to a high-temperature upflow zone. In that case, a resource capacity of >20 MW is likely.

The Akutan Geothermal Project has been touted as a combined heat-and-power project. Kolker (2008) found that if cost-benefit analyses of geothermal vs. diesel generation projects in rural Alaska included direct use of the geothermal fluids, the outcome was substantially more favorable towards geothermal development. This is because heating fuel costs are even higher than the costs of fuel for power generation. Hence, direct uses such as heating, industrial applications, and greenhouse development have been prioritized as components of the Akutan geothermal project.

Without knowing the temperatures of the geothermal reservoir fluid, it is unclear whether a ‘cascaded-use’ approach to geothermal development at Akutan would be feasible. In a ‘cascaded-use’ scenario, fluids pumped to the surface via production wells would first be utilized onsite for power production. Spent fluids from the power plant would then be piped to the village for direct use, and piped back to the ‘reservoir’ area for reinjection (Fig. 28). This would likely require fluids above ~240 °C and with relatively low concentrations of total dissolved solids (TDS) to prevent scaling problems.

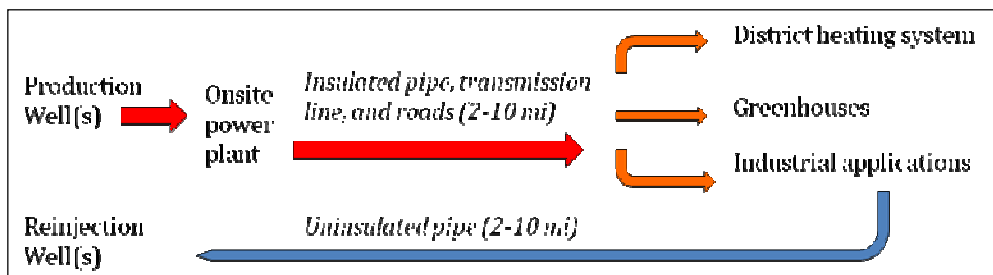


Figure 28. ‘Cascaded-use’ approach to geothermal development at Akutan; feasible only if geothermal production fluids are high-temperature and low-TDS.

The feasibility of the ‘cascaded-use’ approach to development will depend on the temperature, pressure, composition, and location of the production fluids. If production fluids are cooler than C and/or a significant distance from Akutan village, geothermal development at Akutan would have to proceed as presented in Fig. 28. In this scenario, production fluids are simply used onsite for power production, and piped back to the ‘reservoir’ area for reinjection. The direct use applications of geothermal fluids in this scenario are limited to onsite uses such as greenhouses and resort development. Because the multitude of direct use benefits would be sacrificed in that scenario, this could have an impact on project economics since geothermal district heating projects provide a significant monetary benefit to the communities in rural Alaska (Kolker, 2008). Therefore, in that case, it would make sense to drill a dedicated well for direct use applications. This would preserve direct use opportunities such as refrigeration for fish storage and processing, the production of alternative fuels, and other applications.

## V. Conclusions and Next Steps

Results from the 2009 exploration program were successful in terms of building conceptual models of the geothermal resource and siting exploration wells. The most important datasets turned out to be the geochemistry of Akutan hot springs fluids (collected prior to the 2009 study); observations from the geologic reconnaissance, and the results of the MT survey. Together, these results point to a shallow, likely accessible tabular aquifer(s) of 155-220 °C and a deeper, hotter resource of <270 °C that may be inaccessible for development. Two exploratory wells have been sited that would verify the existence of these aquifers, and determine their developability.

The two anomaly areas identified by the remote sensing study are not associated with measured thermal anomalies on the ground and are likely to be related to a surface property like albedo, not elevated temperature related to a geothermal system. At this stage, they are not relevant to our resource evaluation. However, they cannot be completely dismissed as there is slight overlap between those results and the soil geochemistry results. Therefore we have sited lower-priority exploration wells in the general area identified by these studies.

The next step in the Akutan geothermal project is the drilling of 2-4 exploratory wells. Due to the roadless and rugged terrain on Akutan geothermal area, drilling rigs will have to be helicoptered in, which limits the options to small-diameter (“slimhole”) wells. Core, cuttings, P/T data, and other information will be collected from the boreholes during the drilling phase.

Beyond drilling exploratory wells, sampling the fumaroles for gas analyses is of high priority. Gas sampling at Akutan fumaroles was conducted in the 1990’s by USGS (Symonds, 2003); however, the analytic data is not of sufficient quality to be used for geothermal resource evaluation. The gas samples were air-contaminated and several important analyses were omitted (e.g., H<sub>2</sub>). Fumarole samples should be analyzed for gas composition as well as H and O isotopes. The isotopic data be integrated with the other chemical data in order to (1) get an estimate of the temperature of steam separation (boiling) within the reservoir by comparing the <sup>18</sup>O and d contents of the fumarole steam to the hot spring water; and (2) estimate the relative proportions of magmatic, meteoric, and sea water in the samples (D. Rohrs, pers. comm.).

Another high priority for continued resource evaluation and project management is the acquisition of high-resolution imagery over the entire geothermal area. At present, no high-resolution imagery exists for Akutan Island. Such imagery could help with identifying structural features as well as drilling and development logistics. Additionally, further field tests could be done to follow up on the remote sensing results. These include field based thermal imaging, transect thermal profiling, point temperature measurements over a longer time at the identified anomaly area and background area, and other studies.

## References

Cumming, W. and Mackie, R., 2010. Resistivity Imaging of Geothermal Resources Using 1D, 2D and 3D MT Inversion and TDEM Static Shift Correction Illustrated by a Glass Mountain Case History. Proceedings, World Geothermal Congress 2010.

Fournier R.O., 1981. Application of water geochemistry to geothermal exploration and reservoir engineering. *In: Geothermal Systems: Principles and Case Histories*, Ryback and Muffler eds., John Wiley and Sons, NY, 109-143

Fournier R.O., 1989. Lectures on geochemical interpretation of hydrothermal waters. *UNU Geothermal Training Programme, Reykjavik, Iceland*. Report 10, 1989. [www.unugtp.is/solofile/33667](http://www.unugtp.is/solofile/33667)

Giggenbach, W., 1991. Chemical Techniques in Geothermal Exploration. *In: The Application of Geochemistry in Geothermal Reservoir Development*, F. D'Amore Ed. 1991 UNITAR/UNDP Guidebook.

Information Insights, 2010. Akutan Geothermal Energy Demand and Stakeholder Assessment. *Unpublished report to the City of Akutan and the Alaska Energy Authority*, 34p.

Kolker, A., 2008. Geothermal Development in Alaska: A Plan. *Unpublished report to the Alaska Energy Authority*, 26p.

Kolker, A., 2008. Geologic Setting of the Central Alaskan Hot Springs Belt: Implications for Geothermal Resource Capacity and Sustainable Energy Production. *Ph.D. Dissertation, University of Alaska Fairbanks*, 203p. Available Online at: <http://www.uaf.edu/rap/students/Alumni/Kolker-dissertation-2008.pdf>

Lu, Z., C. Wicks, D. Dzurisin, W. Thatcher, and J. Power, 2000. Ground Deformation Associated with the March 1996 Earthquake swarm at Akutan Volcano, Revealed by Satellite Radar Interferometry. *Journal of Geophysical Research*, v. 105, No. B9, p. 21483-21495.

Miller, T.P., G. McGimsey, D. Richter, J. Riehle, C. Nye, M. Yount, and J. Dumoulin, 1998. Catalog of the historically active volcanoes of Alaska. *USGS Open-file Report 98-582*.

Motyka, R., and C. Nye, eds., 1988. A geological, geochemical, and geophysical survey of the geothermal resources at Hot Springs Bay Valley, Akutan Island, Alaska. *Alaska Division of Geological and Geophysical Surveys (ADGGS), Report of Investigations 88-3*.

Motyka, R.J., S. Liss, C. Nye, and M. Moorman, 1993. Geothermal Resources of the Aleutian Arc. *ADGGS Professional Paper 114*.

Newhall, C.G., and D. Dzurisin, 1988. Historical unrest at large calderas of the world. *USGS Bulletin* 1855.

Powell, T., and W. Cumming., 2010. Spreadsheets for Water and Geothermal Gas Chemistry. *Proceedings of the Thirty-Fifth Workshop on Geothermal Reservoir Engineering*, Stanford University, Stanford, California, SGP-TR-188.

Reyes, A.G., Giggenbach, W.F., Saleras, J.R., Salonga, N.D., Vergara, M.C., 1993. Petrology and geochemistry of Alto peak, a vapor-cored hydrothermal system, Leyte Province, Philippines. *Geothermics*, 22, 479-519.

Richter, D.H., C.F. Waythomas, R.G. McGimsey, and P.L. Stelling, 1998. Geology of Akutan Island, Alaska. *USGS Open-File Report 98-135*, 1 sheet, 1:63,360 scale

Symonds, R. B., R. Poreda, W. C. Evans, C. J. Janik, and B. E. Ritchie, 2003. Mantle and crustal sources of carbon, nitrogen, and noble gases in Cascade-Range and Aleutian-Arc volcanic gases. *USGS Open-File Report 03-436*.